MASSACHUSETTS INSTITUTE OF TECHNOLOGY

LINCOLN LABORATORY

CHARGED PARTICLE RADIATION ENVIRONMENT
IN SYNCHRONOUS ORBIT

A. G. STANLEY
J. L. RYAN

Group 63

TECHNICAL REPORT 443

15 MAY 1968

LEXINGTON   MASSACHUSETTS

ABSTRACT

The present state of knowledge of the charged particle radiation environment in synchronous orbit is described. The composition, intensity, energy spectrum and temporal variations of the radiation are listed. The data are based on measurements on board satellites in elliptical and in synchronous orbits, including the results from the electron telescope on board LES-4, whose apogee is in synchronous orbit. The radiation consists mainly of trapped electrons and low energy protons, but solar flare protons also make a significant contribution. The time-averaged data are given in a form useful for predicting the long-term radiation environment to which a satellite in synchronous orbit would be exposed.

iii

CONTENTS

CHARGED PARTICLE RADIATION ENVIRONMENT
IN SYNCHRONOUS ORBIT

I.   INTRODUCTION

This report describes the current state of knowledge of the natural charged particle radiation environment to which a satellite traveling in an earth synchronous orbit would be exposed.   In order to include satellites in quasi-synchronous orbits, the region considered lies between 18,000 and 19,363 nmi.   This may be expressed in other units as shown below.

	Altitude			Radial Distance	Earth Radii
nmi	stat. mi	km		km	(R_o)
18,000	20,718	33,358		39,736	6.23
19,363	22,237	35,884		42,262	6.63

A satellite in synchronous orbit is subject to the following types of natural charged particle radiation: trapped particles, mainly electrons and low energy protons; solar flare particles, mainly protons; and cosmic radiation.   Of these, the trapped particles are by far the most numerous, but solar flare protons make an important contribution, particularly during a sunspot maximum.

For a complete characterization of the radiation environment, the particle flux intensity, direction and energy spectrum should be measured as a function of time, since all these parameters are subject to both short and long term variations.   Ideally, all measurements should be made from satellites in the synchronous orbit.

The ATS 1 satellite, which was launched into the synchronous orbit on 6 December 1966, carries several experiments on board to measure both the proton and electron distribution (see Table I).   Results giving a fairly comprehensive description of the radiation environment in the synchronous orbit are now becoming available.[1-13]   In the absence of such data it was necessary to collate individual measurements from satellites in elliptical orbits as they traversed the synchronous orbit.   The comparison of these results was complicated by temporal variations of the fluxes and by differences in energy response of the various instruments.[14]

In the absence of sufficient data from satellites in the synchronous orbit, measurements obtained from a satellite spending a large fraction of its time in synchronous orbit is of considerable interest.   LES-4 was launched on 21 December 1965 into an elliptical orbit with an apogee near synchronous orbit and a perigee of 200 km.   For 30 percent of its time it was located at $R_o > 6$.   An electron telescope on board the satellite monitored electrons in three integral energy ranges >150 keV, >850 keV and >2.7 MeV.   It also included a proton channel in the range 1.8 to 50 MeV.   The data obtained from LES-4 are compared with other experimental results in this report.

TABLE I			
RADIATION DETECTORS ON BOARD ATS-1 SATELLITE (Ref. 1)			
Organizer	Detector	Particles	Energy Range
Aerospace Corporation	Omnidirectional Spectrometer	Electrons Protons	>300 keV, >450 keV, >1.9 MeV $5-21$ MeV, $21-70$ MeV
University of Minnesota	Proton Electron Spectrometer	Protons and Electrons	$50-150$ keV, $150-500$ keV, $50-1000$ keV
University of California, San Diego	Omnidirectional Particle Detector	Protons Electrons	>12 MeV, >20 MeV >0.5 MeV, >1 MeV
Bell Telephone Laboratories	Multi-element Particle Detecting Telescope	Protons Alpha Particles Electrons	$0.7-100$ MeV $1.8-85$ MeV >1 MeV
Rice University	Suprathermal Ion Detector	Positive Ions Electrons	$0.25-50$ eV >3 keV

II. TRAPPED ELECTRONS

A. Vette and Lucero's Data for Electrons at Synchronous Altitudes

Vette and Lucero[15] have processed data from Explorers 6, 12 and 14, Imp A, OGO-A, and ERS-17 to obtain the most comprehensive information about the electron distribution in the synchronous orbit covering the energy range between 40 keV and 2 MeV and the time range from near solar maximum through solar minimum.

They found that the time-averaged omnidirectional flux for energy greater than E may be expressed by an exponential function

$$J(>E, B/B_o, \Phi) = CA(\Phi) (B/B_o)^{-b} E^{N(\Phi)} \exp[-E/E_o] \text{ e/cm}^2 \cdot \text{sec} \qquad (1)$$

for energies greater than 10 keV, where

> B = the geomagnetic field,[16,17]
>
> B_o = the B-coordinate at the magnetic equator
>
> Φ = local time in hours
>
> C = 9×10^7 at solar minimum and 4.5×10^7 at solar maximum with an estimated error of 2
>
> b = 0.625
>
> E_o = 0.215 MeV

and A and N are functions of the local time. A more useful presentation of the integral spectrum averaged over local time at solar minimum is shown in Fig. 1. At energies above 0.5 MeV this spectrum may be expressed in the form

$$J(>E, B/B_o) = 5.04 \times 10^7 (B/B_o)^{-0.625} \exp[-E/0.215] \text{ e/cm}^2 \cdot \text{sec} \quad . \quad (2)$$

At lower energies the flux increases above the value given by Eq. (2). Table II shows the average omnidirectional flux at the magnetic equator ($B/B_o = 1$) at solar minimum. The figures are believed to be accurate within a factor of two. The probability that the flux will exceed the average flux has also been computed, but for missions with a duration in excess of several weeks, the average flux should be used. W. D. Brown[19] has compared Vette and Lucero's model to minimum and maximum flux rates measured by Aerospace Corporation on ATS-1 in synchronous orbit, as shown in Fig. 2. The combined Explorer 12 and 14 spectra are also shown. Considering the factor of 2 uncertainty in Vette and Lucero's time-averaged environment, the curves are in good agreement.

TABLE II						
TRAPPED ELECTRON FLUX						
		Average Omnidirectional Flux (e/cm^2 · sec) $B/B_a = 1$, Sunspot Minimum (Ref. 15)				Minimum Shielding to Stop Electrons of Energy E_1 (in Al, Ref. 18) (mg/cm^2)
		L = 6.6, 19,363 nmi		L = 6.0, 17,300 nmi		
Energy Range (MeV)		Integral $(E > E_1)$	Differential $(E_1 < E < E_2)$	Integral $(E > E_1)$	Differential $(E_1 < E < E_2)$	
E_1	E_2					
0.01	0.02	6.51×10^7	7.1×10^6	5.69×10^7	2.2×10^6	0.25
0.02	0.05	5.80×10^7	1.15×10^7	5.46×10^7	6.1×10^6	0.85
0.05	0.10	4.65×10^7	1.15×10^7	4.85×10^7	8.9×10^6	4.3
0.10	0.20	3.50×10^7	1.40×10^7	3.96×10^7	1.30×10^7	14.1
0.20	0.40	2.10×10^7	1.31×10^7	2.66×10^7	1.47×10^7	41.8
0.40	0.60	7.94×10^6	4.87×10^6	1.19×10^7	6.5×10^6	158
0.60	0.80	3.07×10^6	1.88×10^6	5.37×10^6	2.96×10^6	210
0.80	1.00	1.19×10^6	7.2×10^5	2.41×10^6	1.33×10^6	309
1.00	1.20	4.66×10^5	2.84×10^5	1.08×10^6	5.9×10^5	424
1.20	1.40	1.82×10^5	1.11×10^5	4.87×10^5	2.68×10^5	530
1.40	1.60	7.14×10^4	4.34×10^4	2.19×10^5	1.21×10^5	636
1.60	1.80	2.80×10^4	1.70×10^4	9.83×10^4	5.41×10^4	742
1.80	2.00	1.10×10^4	6.7×10^3	4.42×10^4	2.44×10^4	848
2.00	2.50	4.32×10^4	3.90×10^3	1.98×10^4	1.71×10^4	954
2.56	3.00	4.18×10^2	3.77×10^2	2.69×10^3	2.33×10^3	1220
3.00	3.50	4.06×10	3.66×10	3.63×10^2	3.14×10^2	1490
3.50	4.00	3.95	3.57	4.92×10	4.25×10	1750
4.00	5.00	3.84×10^{-1}	3.80×10^{-1}	6.66	6.54	2010
5.00		3.64×10^{-3}		1.22×10^{-1}		2540

B. LES-4 Data

Energetic particle fluxes were measured by an experiment aboard LES-4. This instrument consists of several surface barrier transmission detectors stacked and operated with coincidence techniques in order to identify particle nature and energy. The response of the various channels to monoenergetic electrons was measured as a function of energy. The criterion for selection of threshold energy was minimum change in effective efficiency with spectral characteristic energy. Only 3 channels will be considered at this point with selected thresholds at 150 keV, 850 keV, and 2.75 MeV.

The omnidirectional flux has been obtained by suitable averaging of directional measurements.

The low energy channel has been corrected for bremsstrahlung while coincidence techniques eliminate the problem in the upper channels. The >2.75 MeV channel has been corrected for galactic cosmic rays penetrating the shielding.

Points consisting of 5-minute averages were found for every observed passage of LES-4 through the L = 6.6 region from launch through the next 747 days. The average over these 56 points is plotted in Fig. 3. Both local time and magnetic storm effects should be smoothed because of random sampling. B/B_o ranged from 1.3 to 5 in these samples.

Also plotted are spectra from the points in which the 850 keV channel had both its maximum and minimum count at L = 6.6.

Comparison of these results to those shown in Fig. 2 indicate quite good agreement.

C. Variation of Electron Flux with L

It is desirable to ascertain the variation of the electron flux and of the energy spectrum with geocentric equatorial distance R_o for satellites in a quasi-synchronous orbit.

If the earth's geomagnetic field were that of a perfectly centered dipole, the magnetic shell L in the L, B coordinate system developed by McIlwain[16,17] should be equal to R_o measured in units of earth radii. In the vicinity of the earth's synchronous orbit, the geomagnetic field is disturbed by magnetic storms and the steady state solar wind and undergoes both diurnal and other irregular temporal variations.[20,21] The location of the L-shell is then no longer fixed but varies with changes in the earth's magnetic field. The experimental data should therefore be more properly plotted against R_o, but in this report the parameter L will be retained following the sources from which the data have been obtained.

Figure 4 shows the average and the maximum omnidirectional flux at L = 6.0, L = 6.6 and L = 7.0. The results are based on calculations by J. I. Vette on OGO-A spectrometer data in the energy range from 50 to 690 keV obtained by Winckler and Pfitzer of the University of Minnesota.[22-26] The average values at L = 6.6 and L = 7.0 show an enhancement of the low energy electron flux in excess of the exponential spectrum. The energy spectrum softens with increasing L.[27] The average omnidirectional flux at L = 6.0 may be approximated to an exponential spectrum of the form

$$J(>E) = 5.91 \times 10^7 \ e^{-E/0.25} \ e/cm^2 \cdot sec \quad . \tag{3}$$

The constant 5.91×10^7 has been normalized for the average flux at the magnetic equator at solar minimum by comparison with the constant of Eq. (2). Values of J for L = 6 are also shown in Table I.

Figure 5 is a comparison of the variation of electron flux with L from data obtained by Explorer 14 (Ref. 15) and LES-4. The Exp. 14 data have been corrected to local noon and represent the median values over the lifetimes of the data. The LES-4 data are simple means over the data at different L values. The B/B_o and local time variation is similar for different L's.

Since a very definite variation with L occurs it should be pointed out that a geostationary satellite would be expected to experience an average flux dependent on the longitude at which the satellite is fixed. The variation in L with longitude is shown in Fig. 6.

D. Temporal Variations

The flux level of the outer zone electrons varies in time by about two orders of magnitude. As an example, Fig. 7 indicates the values of the fluxes of >150 keV and >850 keV electrons as sampled by LES-4 at L = 6 over a period of 200 days. The detectors on board the ATS-1 satellite have provided detailed information on these variations.[1-13,28]

1. Diurnal or Local Time Variations

The distortion of the geomagnetic field in the synchronous orbit by the solar wind produces an average diurnal variation in the electron intensity.[29] The particles at midnight are on particle shells which lie outside those sampled at noon and hence have a lower particle intensity. The magnitude of the variation is a function of the electron energy with the largest decreases in flux on the night side appearing for the high energy electrons. The electron spectrum is softer at night than during the day.

During quiet and moderately disturbed conditions the maxima and minima in the range from 300 to 1900 keV are displayed about an hour ahead of local noon and midnight.[4,5] On the other hand, Freeman and Maguire[28] found that thermal plasma ions show maximum fluxes in the midnight to dawn sector.

During quiet times there is a smooth diurnal variation which becomes less smooth as magnetic activity increases. During more disturbed times, the satellite leaves the region of stable trapping on the night side and enters a part of the magnetosphere which is inhabited by rapidly fluctuating electron populations.[3] On some occasions, typically following a magnetic storm, no diurnal variation is found; instead the flux increases in a stepwise fashion throughout the post storm recovery period.

Typical diurnal changes during quiet or moderately disturbed periods are as follows:[2]

	Maximum Variation	Minimum Variation
$E \geqslant 300$ keV	3	1.5
$E \geqslant 450$ keV	3.5	1.5
$E \geqslant 1050$ keV	9	3
$E \geqslant 1900$ keV	20	3

The variations are not correlated to K_p.[5]

Before the results from the ATS-1 satellite became available Vette and Lucero[15] adopted an iterative procedure to obtain from all their data the composite local time variation shown in Fig. 8. Measurements of the local time variation reported earlier by Frank[29,30] are included. The figure shows that the local time variation increases with energy and peaks around 9 o'clock with a minimum at midnight. The range of variations of the data obtained from ATS-1 appears to be somewhat smaller than that of the data from elliptical orbits. This is mainly due to

differences in data selection and analysis.[5] The data obtained during very disturbed days have been omitted in the analysis of ATS-1 results.

2. Short Term Changes

Some small scale periodic fluctuations of electron fluxes, with a period of $100 - 1000$ seconds depending on the energy, are associated with the longitudinal drift of bunches of electrons that have been injected into the magnetosphere.[13]

During magnetic storms the electrons >45 keV may also undergo quasi-regular or irregular modulations by one order of magnitude with a typical period of six minutes.[31]

3. Variations Due to Magnetic Storms

At $L = 4$ there is a strong correlation of electron flux with magnetic storms. Each large flux increase is accompanied by an increase of spikiness of K_p. An initial decrease in flux at the onset of the storm is followed by a rapid rise during the main phase of the storm by about two orders of magnitude with a rise time of 10 minutes or longer depending on the energy. A slow exponential decay then sets in which continues until the onset of the next storm.[32]

In the synchronous orbit the electron flux is also affected by conditions on the sun, but the variations are far more irregular and do not correlate well with magnetic storms. This is believed to be due to physical motion of the magnetospheric boundary.[9] Electrons in the energy range $50 - 150$ keV show large increases of intensity that persist for $30 - 90$ minutes and repeat with a period of $2 - 4$ hours. The largest intensity occurs in the midnight to dawn sector.[10]

Energetic electrons show a greater response than the low energy ones. Electrons >1.9 MeV decrease by one order of magnitude disappearing at local midnight. This is followed by a gradual recovery which takes place more slowly than for low energy electrons.[3]

Occasionally, the synchronous altitude moves right outside the magnetosphere, usually within three hours of local midnight. Subsequently discrete clouds of energetic particles are detected which execute repeated longitudinal drifts about the earth, as well as bursts of very low energy, $E < 50$ keV, highly directional positive ions.[7]

4. 7-Day and 27-Day Variations

A near periodic 7-day recurrence of flux depressions has been observed[3] similar to the low altitude variations related by Williams[3] to changes in the interplanetary field direction.

Magnetic activity, and hence the electron flux in the synchronous orbit, has a tendency to recur after the lapse of one or more intervals of 27 days, the approximate period of rotation of the sun relative to the earth moving along its orbit.[33] The 27-day variations can persist for long time periods like a year but are not always present.

5. Variation with Solar Cycle

Vette and Lucero[15] found no evidence for an increase in the trapped radiation flux levels at $L = 6.6$ as solar maximum is approached. Their data showed a decrease by a factor 2, which is within the intercomparison accuracy of the various satellite measurements. This is an agreement with O'Brien's observation[34] that the range of intensities of the outer zone electrons in 1963 was the same as in 1959, even though the solar activity strongly influences the outer zone intensities via magnetic storms. Presumably, the principal effect of the solar maximum vs solar minimum

will simply be an increase in frequency (and to a lesser extent in magnitude) of changes of the outer zone.

Frank and Van Allen[35] found that the inner edge of the outer radiation belt moved outward during the declining phase of solar activity cycle 19. The changes produced by this effect in the spectral distribution of the electron flux at L = 6.6 appear to be within the margin of error of different experimental observations.

The LES 4 instrument sampling in the synchronous region shows no indication of a dependence of flux levels on solar activity. Data examined include some 800 days of operation, wherein the smoothed sunspot number changed from 20 (near its minimum value) to 100 (above the maximum of the mean of sunspot cycles 1 through 19).

E. Pitch Angle Distribution

The pitch angle distribution determines the direction from which the trapped charged particles will strike a satellite in orbit. The pitch angle is a function of the particle energy and undergoes temporal variations like all the other parameters.

Pitch angle distributions for electrons in the synchronous orbit have been reported by Lezniak et al.[6] The distribution at local noon during a disturbed period is shown in Fig. 9. The low energy distribution is highly anisotropic. Similar measurements are believed to have been carried out by Pfitzer and Winckler on OGO A.[23-26] The measurement may be made with a single directional detector if the satellite spin axis is perpendicular to the magnetic field. Otherwise a series of directional detectors are required covering the quadrant from 0 to 90°. The direction of the spin axis must be known with respect to the magnetic field. In the synchronous orbit the pitch angle distribution cannot be derived from the omnidirectional intensity along a line of force, since the adiabatic invariance conditions are not obeyed.[36]

F. Low Energy Electrons

Frank[37-39] measured the intensity of electrons in the range from 200 eV to 50 keV near the magnetic equator with an array of electrostatic analyzers on OGO-3. The electron energy densities remained fairly constant at 3×10^{-8} erg/cm^3 over $L \simeq 4.0 - 7.5$[37] corresponding to an integral electron flux >200 eV on the order of 10^9 e/cm$^2 \cdot$ sec. This is in good agreement with an integral electron flux >610 eV of 3×10^9 e/cm$^2 \cdot$ sec at a geocentric distance of 8 R$_o$ (Fig. 6, Ref. 24). At higher energies the flux varies considerably with radial distance (Fig. 1, Ref. 38). The differential energy spectrum decreases monotonically with energy at L = 3.9 (Fig. 10, Ref. 39), whereas at 10.1 R$_o$ it shows a broad peak at 2 keV (Fig. 8, Ref. 38). No spectral data have been published closer to the synchronous orbit.

Earlier measurements of low energy electrons at L = 6.6 were made by Freeman[40,41] on Explorer 12 using cadmium sulfide total energy flux detectors and also by Russian experimenters on Zond 2[42] and Mars 1[43] employing charged particle traps. Their results were more qualitative in nature, but are in broad agreement with Frank's data.

Serbu and Maier[44-46] have measured the electron distribution from 0 to 100 eV near the geomagnetic equatorial plane by means of retarding potential analyzers on IMP-1 and -2. The electrons and positive ions below 4 eV constitute a neutral thermal plasma with a Maxwell-Boltzmann energy distribution. In the synchronous orbit the electron density is in the 25 to 80 e/cm^3 range and the electron temperature lies between 1 and 2 eV. The electron flux in

the $0 < E < 5\,eV$ energy range was found to be $3 \times 10^9\,e/cm^2 \cdot sec$ on IMP-1. There is also a higher energy component whose flux in the $5 < E < 10\,eV$ energy range is $2 \times 10^8\,e/cm^2 \cdot sec$.[45]

Slysh[47] has derived the plasma density from antenna impedance measurements on Zond-2. He obtained a density of $100\,e/cm^3$ at $6\,R_o$ and a radial dependence

$$N_e = 1.3 \times 10^5\,R_o^{-4}$$

valid from 4 to $7\,R_o$ in good agreement with the results of Serbu and Maier.

III. TRAPPED PROTONS

A. Intensity and Energy Distribution

The positively charged trapped particles in the outer radiation zone consist predominantly of low energy protons. Van Allen and Krimigis[48,49] have recently found trapped alpha particles with a maximum intensity at $L \sim 3.1$. The ratio of the differential spectral intensity of alpha particles to that of protons is of the order of 0.05 at 2 MeV, and the ratio of the integral directional intensities $(E > 0.52\,MeV/nucleon)$ is 2.3×10^{-4}.

Proton measurements in the synchronous orbit were made by Davis and Williamson[50-52] on Explorers 12 and 14, by Vernov, et al.,[53] on Cosmos 41 and by Krimigis and Armstrong[54] on Mariner 4.

Davis and Williamson measured protons in the energy range from 100 keV to 4.5 MeV with a directional scintillation counter. Vernov, et al., used semiconductor counters sensitive to protons in two ranges, $0.4\,MeV < E < 7\,MeV$ and $3\,MeV < E < 8\,MeV$. Krimigis and Armstrong also measured protons in two energy ranges, $0.50 \leqslant E_p \leqslant 11\,MeV$ and $0.88 \leqslant E_p \leqslant 4\,MeV$ on the geomagnetic equator. The experimental data of Davis and Williamson have been processed by J. H. King[55] of Aerospace Corporation, together with data from proton measurements in lower orbits which cover the energy range from 400 keV to 4 MeV. From these data a model of the proton environment has been constructed which gives the omnidirectional flux for energy greater than E MeV,

$$J(>E, B, L) = F(B, L)\,exp\,[(0.4 - E)/E_o(B, L)]\,p/cm^2 \cdot sec \qquad . \qquad (4)$$

Figure 10 shows the energy distribution of the protons at $L = 6.6$ as a function of B/B_o. The values of the distribution function F and the spectral function E_o at the magnetic equator are:

	$L = 6.6$	$L = 6.0$
$F(B_o, L)$	$4.00 \times 10^5\,p/cm^2 \cdot sec$	$1.6 \times 10^6\,p/cm^2 \cdot sec$
$E_o(B_o, L)$	$0.111\,MeV$	$0.112\,MeV$

Calculations by J. I. Vette on experimental data by Davis and Williamson extend the proton distribution down to 100 keV as shown in Fig. 11. There is a significant enhancement of the flux at energies below 250 keV over the exponential distribution. Table III shows the average omnidirectional flux at the magnetic equator obtained from Eq. (4) for energies above 400 keV and from Fig. 11 for energies between 100 and 400 keV. The accuracy of the proton model environment is estimated to be within a factor of two for $L \leqslant 4.5$. Larger amplitude temporal variations and a relative shortage of data decrease the accuracy at synchronous orbit.

		Omnidirectional Flux (p/cm² · sec) $B = B_a$				Minimum Shielding to Stop Protons of Energy E_1 (in Cu, Ref. 56) (mg/cm²)
Energy Range (MeV)		L = 6.6, 19,363 nmi		L = 6.0, 17,300 nmi		
E_1	E_2	Integral ($E > E_1$)	Differential ($E_1 < E < E_2$)	Integral ($E > E_1$)	Differential ($E_1 < E < E_2$)	
0.10	0.25	1.2×10^7	1.0×10^7			0.16
0.25	0.50	1.7×10^6	1.5×10^6			0.51
0.50	0.75	1.6×10^5	1.5×10^5	6.4×10^5	5.9×10^5	1.45
0.75	1.00	1.7×10^4	1.4×10^4	6.8×10^4	6.1×10^4	2.8
1.00	1.25	1.7×10^3	1.5×10^3	6.8×10^3	6.1×10^3	4.5
1.25	1.50	1.8×10^2	1.5×10^2	7.1×10^2	6.4×10^2	6.75
1.50	1.75	1.8×10	1.6×10	7.1×10	6.3×10	8.1
1.75	2.00	1.9	1.7	7.7	6.9	11.5
2.00	2.25	1.9×10^{-1}	1.7×10^{-1}	7.7×10^{-1}	6.9×10^{-1}	14.5
2.25	2.50	2.0×10^{-2}	1.8×10^{-2}	8.0×10^{-2}	7.1×10^{-2}	17.5
2.50	2.75	2.2×10^{-3}	2.0×10^{-3}	8.7×10^{-3}	7.8×10^{-3}	21
2.75	3.00	2.2×10^{-4}	2.0×10^{-4}	8.7×10^{-4}	7.9×10^{-4}	24.5
3.00		2.1×10^{-5}		8.4×10^{-5}		28

B. Temporal Variations

During magnetic storms, changes occur in the proton intensity with apparent temporary enhancement of proton flux during the main phase. At L-values between 5 and 8, large time variations do occur for protons with energies greater than 1 MeV, but protons near 100 keV are relatively more stable.[27]

Davis and Williamson[52] (Fig. 12) show the effect of a solar event on 5 October 1962. High energy protons >970 keV are sufficiently enhanced to produce a separate peak at L = 5.8. The >520-keV protons are also enhanced, whereas the >141-keV protons are only slightly disturbed. Six days later the enhancements have decayed. The proton buildup is coincident with high latitude negative bays.

Data obtained from Explorer 14 (Fig. 13) show that above 1.7 MeV the proton intensities fluctuate by at least one order of magnitude at L = 6, whereas low energy proton intensities are much more stable. Davis and Williamson[52] compared the proton intensities measured in 1965 with those measured in 1962. They found that the intensity of protons above 1.7 MeV throughout the region from L = 2.5 to 5 was larger by a factor of two to three in 1965. The enhancement extended to energies down to 500 keV, whereas 100 to 300 keV protons were greatly depleted. Also, the 1962 Davis-Williamson data (>0.5 Mev) are in apparent disagreement with the data obtained in 1964 on Mariner 4. The latter is about two orders of magnitude smaller than the former for L $\geq$ 6.0.[55]

Freeman and Maguire[28] have made a detailed study of the temporal variations of low energy protons in the synchronous orbit. During periods of moderate magnetic activity, a high particle flux is seen near local midnight and the particle intensities after midnight are higher than those before midnight. During periods of high magnetic activity, the particle fluxes undergo large local time variations. The enhanced particle flux distribution extends over a larger fraction of the night-side portion of the synchronous orbit and the pre and postmidnight asymmetry is somewhat reduced.

C. Pitch Angle Distribution

Davis[51] has measured the equatorial pitch angle (EPA) distribution at L = 6 for proton energies of 97 and 495 keV (Fig. 14). The distribution is fairly isotropic with a maximum at 90° and is subject to temporal variations. Data obtained on different passes show even larger discrepancies, particularly for protons with energies greater than 495 keV.

D. Low Energy Protons

Frank[37,39] measured the low energy proton distribution near the magnetic equatorial plane in the range $200 \, \text{eV} \leqslant E \leqslant 50 \, \text{keV}$ with an array of sensitive electrostatic analyzers mounted on OGO-3. The omnidirectional proton intensity at L = 6 in the energy range $1.8 \leqslant E \leqslant 48 \, \text{keV}$ was found to be $2(\pm 1) \times 10^8 \, \text{p/cm}^2 \cdot \text{sec}$. The proton energy density at L = 6.5 in the range $190 \, \text{eV} \leqslant E \leqslant 48 \, \text{keV}$ is $3.9 \times 10^{-8} \, \text{erg/cm}^3$ at a geomagnetic latitude of 22°. This is about 4 times the energy density observed by Davis[51] for protons of energy $\geqslant 97 \, \text{keV}$.

The above data represent quiet-time conditions. During the main phase of a geomagnetic storm the proton intensities at L = 6 to 6.5 in the energy range $200 \, \text{eV} \leqslant E \leqslant 50 \, \text{keV}$ increase by a factor 2 to 2.5. The proton angular distributions during the storm were found to be almost isotropic with maximum directional intensities at an equatorial pitch angle of 90° (Ref. 23).

The proton differential energy spectrum at L = 6.0 and 6.6 is shown in Fig. 15. The data were obtained from Figs. 5, 6, 7 and 11 of Frank's paper[39] and include higher energy values calculated by Frank from the integral energy spectrum at L = 6.0, EPA = 65° published by Davis.[51] The following features are worth noting:

A very good fit of Frank and Davis' data at higher energies despite an interval of almost 3 years between the measurements.

At about 1 keV the proton flux decreases below background response of the instrumentation.

Below 1 keV the proton flux decreases as L increases, whereas above 10 keV the opposite is true.

Serbu and Maier[46] have measured the distribution of positive ions from 0 to 45 eV by means of a retarding potential analyzer on IMP-2. The positive ions have a Maxwell-Boltzmann energy distribution with a temperature of about 3 to 5 eV at a geocentric distance from 5 to 7 earth radii. The density of positive ions in this region declined rather sharply from $300/\text{cm}^3$ at $R_E = 5$ to $20/\text{cm}^3$ at $R_E = 7$.

The Rice University ion detector aboard the ATS-1 satellite has measured a highly directional flux of positive ions moving with a bulk flow velocity of 30 km/sec toward the sun. During one event the alpha/proton density ratio was approximately 3%, the proton density 6 protons/cm^3 and the temperature 1 eV.[8]

Ion mass spectrometer measurements on OGO-A[57] have yielded a ratio of 100 to 1 in the He^+ to H^+ concentrations over a range of altitudes from 1500 to 30,000 km.

IV. SOLAR FLARE PARTICLES

A. Solar Flares

Solar flares occur in a limited region of the chromosphere, usually in the vicinity of an active sunspot group. The phenomena produced by a solar flare as observed from the vicinity of the earth may be divided into simultaneous and delayed effects as shown in Table IV.[58,59]

TABLE IV			
SOLAR FLARE EFFECTS			
Effect	Energy	Type	Travel Time
Simultaneous			8. 3 minutes
Visible Light			
Radio Waves			
Ultraviolet and X-rays			
Delayed			
Solar Cosmic Ray Particles	10 MeV − >1 GeV	Mainly protons	
Direct			<1 hour
Indirect			20 minutes to 20 hours
Magnetic Storm Particles			20 to 50 hours
Energetic Storm Particles	100 keV − 10 MeV	Mainly protons	
Solar Flare Plasma	10 eV − 100 keV	Ions and electrons	

The importance of a solar flare is defined in terms of the area occupied by the flare at the time of maximum brightness.[60] The most important solar flares (importance classes 3 and 3+) occur very rarely, last for periods up to 8 hours and contribute most of the solar particles. Conversely, flares of importance 1 to 1− (subflares) occur very frequently, have durations of the order of minutes and usually do not contribute any significant particle fluxes.

Most of the largest solar flare events produce direct cosmic ray particles, i.e., particles from a fairly well-defined source in the general vicinity of the sun. The time of arrival of the particles is commensurate with rectilinear travel from the sun and the intensity increases to its maximum value in 3 to 20 minutes. The indirect radiation is isotropic in nature and possesses a steeper energy spectrum; also, the travel time, the rise to peak intensity and the decay take far longer. In many events only indirect radiation is observed.[59] The energetic storm particles do not arrive in appreciable numbers until about a day after a solar flare and reach a maximum at the time of arrival of the magnetic storm at the earth which coincides with the arrival of the solar flare plasma.

B. Composition

1. Positively Charged Cosmic Ray Particles

The composition of solar cosmic rays has been reviewed by Biswas and Fichtel.[61] The primary radiation outside the atmosphere consists predominantly of protons, but also contains alpha particles and heavy nuclei. The energy spectrum of the flare particles varies with each solar event and also over the course of a given event. The low energy spectrum is further influenced by the geomagnetic cutoff at the measuring point and by interaction with the atmosphere if the measurement is made on the ground or at low altitudes.

The Solar Proton Manual[62] states that, at least for proton energies > 30 MeV, the average differential energy spectrum over the course of an event may be expressed in the form

$$\frac{dJ}{dE} = KE^{-n_o} \qquad 3.5 < n_o < 5 \quad .$$

(5)

Freier and Webber[63] have shown that a better representation, not only for protons but also for alpha particles and medium nuclei with $A/Z = 2$, is given by an exponential rigidity spectrum

$$\frac{dJ}{dP} = J_o(A, Z, t) \exp\left[-P/P_o(A, Z, t)\right]$$

(6)

where P is the magnetic rigidity, or momentum per unit charge $= m_o vc/Ze$, which is related to the kinetic energy E (in electron volts) by[64]

$$P^2 Z^2 = E^2 + 2m_o c^2 E$$

(7)

Ze = particle charge

A = atomic number

t = time

m_o = rest mass

v = velocity

c = velocity of light   .

For protons, $m_o c^2 = 938$ MeV   .

P_o lies in the range from 50 to 200 MV; J_o varies from 10^2 to 10^4 p/cm$^2 \cdot$ sec for solar protons.[65] This spectrum applies down to rigidities of 0.2 GV.[66] Both the constant K and the characteristic rigidity P_o vary in a systematic manner during the course of an event. In most events there is an exponential rise to a maximum intensity I_{max} followed by a slower exponential decay. The integrated intensity above a given energy may then be calculated from[67]

$$J(>E) = \int_{-\infty}^{O} I_{max}(>E) \exp(-t/t_R) \, dt + \int_{O}^{\infty} I_{max}(>E) \exp(-t/t_D) \, dt$$

(8)

where $t = 0$ is the time of the peak intensity, t_R and t_D are characteristic rise and decay times which are energy dependent and vary from several hours to several days in different events. The quantity t_R depends on the location of the flare on the sun; t_D is influenced more by general interplanetary conditions. The ratio of t_D/t_R varies from 1.6 to 6 with an average of 4.[68]

12

The integrated intensities also exhibit exponential rigidity spectra of the form[69]

$$F(>E) = G \exp [-P(E)/P_o] \quad . \qquad (9)$$

The characteristic integrated rigidity P_o is close to, but slightly smaller than, that of the spectrum at peak intensity. The solar protons produced by the flare of 23 February 1956 exhibited a P_o of 260 MV. With this exception P_o varies from 50 to 200 MV. Webber[67] plotted the number of events having a P_o greater than a given rigidity P as a function of P for all major events from 1956 to 1962. This is shown in Fig. 16. The linear relationship indicates that P_o varies randomly with a constant probability density and a mean value of 97 MV.[69] There is no correlation between P_o and the total integrated flux or the flare location on the sun's surface.

Alpha particles and heavier nuclei possess approximately the same rigidity spectrum as the protons. The ratio of protons to alphas above a fixed rigidity lies most commonly between one and two although events with ratio greater than 50 have been observed. Webber[65] has observed a correlation between the proton/alpha particle ratio and the characteristic rigidity P_o as shown in Fig. 17. The ratio increases with P_o. A similar correlation between this ratio and the cosmic particle energies was noted by Sakurai.[70] All the heavy nuclei appear to have the same spectral shape and relative abundances shown in Table V taken from the review by Biswas and Fichtel[61] which also shows the corresponding figures for galactic cosmic rays. Among the heavier nuclei carbon 6, nitrogen 7, oxygen 8, and neon 10 are the most abundant.

TABLE V		
(Ref. 61)		
RELATIVE ABUNDANCES OF NUCLEI NORMALIZED TO BASE OF 1.0 FOR OXYGEN ENERGY RANGE: 42 – 135 MeV/NUCLEON		
Element	Solar Cosmic Rays	Galactic Cosmic Rays (10 to 30% uncertainty)
^{2}He	107 ± 14	48
^{3}Li	—	0.3
^{4}Be – ^{5}B	< 0.02	0.8
^{6}C	0.59 ± 0.07	1.8
^{7}N	0.19 ± 0.04	≤ 0.8
^{8}O	1.0	1.0
^{9}F	< 0.03	≤ 0.1
^{10}Ne	0.13 ± 0.02	0.30
^{11}Na	—	0.19
^{12}Mg	0.043 ± 0.011	0.32
^{13}Al	—	0.06
^{14}Si	0.033 ± 0.011	0.12
^{15}P – ^{21}Sc	0.057 ± 0.017	0.13
^{22}Ti – ^{28}Ni	≤ 0.02	0.28

Very small quantities of deuterons and tritons have also been observed, probably 10^{-3} or less of the proton abundance.

M. V. K. Apparao, et al.,[71] have detected 150 solar neutrons/$m^2 \cdot$ sec $\cdot$ sr with energy between 20 and 160 MeV. The main source of neutrons is the neutron albedo generated by knock-on collisions of solar flare and cosmic ray energetic particles with atmospheric particles over the magnetic poles. About 10 percent of all neutrons generated in this way escape into space. This resulted in albedo neutron fluxes in synchronous orbit during 1967 of 8.6×10^3 n/$cm^2 \cdot$ day in the absence of solar activity and of 1.72×10^4 n/$cm^2 \cdot$ day during solar flares.[19] These values are comparable to the solar neutron intensity measured by Apparao, et al.

2. Magnetic Storm Particles

The magnetic storm particles may be divided into two major rigidity groups with an exponential rigidity spectrum [Eq. (6)] and with the following parameters:[65]

	Characteristic Rigidity P_o	Flux J_o
Energetic Storm Particles	5 to 30 MV	10^5 to 10^7/$cm^2 \cdot$ sec
Solar Flare Plasma	0.5 to 2 MV	10^9/$cm^2 \cdot$ sec

The energetic storm particles are thus far more numerous than the solar cosmic rays, but possess far lower energies. At 10 MeV the two particle populations have approximately equal intensities. The energetic storm particles consist mainly of protons, but their exact composition is yet to be determined. Considerable numbers of electrons are also associated with magnetic storms (see below).

Energetic storm particles with the same rigidity spectrum but with very much lower intensity (J_o from 10 to 10^3 particles/$cm^2 \cdot$ sec) are also observed during small magnetic storms which recur over many 27-day cycles of the solar rotation period.[72] A major solar flare starts each series of recurrent events. Bartels[73,74] postulated that these storms are produced by plasma streams which are continuously emitted from long-lived regions of the sun called M-regions.[75] Long-lived solar plasma streams with a 27-day structure were observed by Mariner II.[76] The recurrent storm particles are produced over a period of 1 to 2 days with the intensity increasing and then decreasing more or less symmetrically in time about the time of peak intensity. They consist mainly of protons, but helium nuclei are also present.[77]

3. Electrons

Energetic electrons are very rare, much less than one percent of the protons at 1 MeV. Relatively large fluxes of low energy electrons (<1 MeV) have been observed. Peak fluxes of up to 40,000 e/$cm^2 \cdot$ sec of energy greater than 40 keV have been measured in interplanetary space following solar chromospheric flares.[78] The electrons belong to two classes: prompt electrons which arrive within an hour of the flare and delayed electrons which appear at earth about 20 to 40 hours following a large solar flare and are present from 8 to 24 hours. The propagation of energetic solar flare electrons is usually highly anisotropic and takes place in cones of propagation; outside the boundaries of these cones, the electron flux is much reduced. The cones of the prompt electrons possess opening angles of either 30° (simple events) or 90° (complex events). The buildup time of the prompt electron is less than one hour; the delay time is of the order of a day. The delayed electrons >0.5 MeV possess comparable peak intensities.

14

4. X-Rays

DeJager[79] has suggested one classification of solar x-rays by energy:

Soft x-rays	$\lambda > 1 \overset{\circ}{A}$ or	$E < 10\,keV$
Hard x-rays	$\lambda < 1 \overset{\circ}{A}$ or	$E > 10\,keV$

and another by the mechanism of origin:

Quasi-thermal x-rays emitted by a hot, stationary plasma (up to $10^7\,°K$)

Nonthermal x-ray bursts due to the acceleration of energetic jets of charged particles

Gamma rays of nuclear origin.

No solar gamma rays have been detected. An upper limit for the flux of gamma rays above 50 MeV is 10^{-2} photons/$cm^2 \cdot$ sec.[80] The nonthermal bursts consist of short-lived bursts of hard x-rays (10^4 to $10^6\,eV$) with durations ranging from a few seconds to a few minutes and with an energy flux up to 2×10^{-5} ergs/$cm^2 \cdot$ sec.[81-86] The spectral shape appears to be independent of intensity and decreases rapidly from 20 to 150 keV.[86]

Solar flares are also accompanied by changes in intensity and spectral composition of the quasi-thermal x-rays emitted by the solar corona which are summarized in Table VI taken from the review article by Mandelstam.[87] Thermal x-rays may be divided into a quasi-stable component emitted by undisturbed coronal regions and a slowly varying component emitted by active regions. Below about 20 $\overset{\circ}{A}$ the spectrum is continuous and mainly determined by the slowly varying component. Between 20 and 100 $\overset{\circ}{A}$ the contributions of the two components are roughly equal and a line spectrum produced by elements present in the corona is superimposed on the continuous spectrum. The disturbed corona subjects the intensity below 20 $\overset{\circ}{A}$ to considerable variations over periods of a few days and up to several months. Disturbed and undisturbed conditions are also correlated to periods of maximum and minimum solar activity. During class 2-3 solar flares, the boundary of the spectrum is displaced down to about 1 to 0.1 $\overset{\circ}{A}$ and the flux below 10 $\overset{\circ}{A}$ rises by an order of magnitude. The total flux below 100 $\overset{\circ}{A}$ increases by a factor 2. Figure 18, taken from an article by H. H. Malitson,[88] shows the x-ray spectrum down to 1 $\overset{\circ}{A}$ under different solar conditions.

TABLE VI SOLAR X-RAYS (Ref. 87)		
λ (Å)	Quiet Sun (erg/$cm^2 \cdot$ sec)	Flores (erg/$cm^2 \cdot$ sec)
$\leqslant 10$	10^{-5} to 10^{-3}	10^{-2}
$\leqslant 20$	10^{-4} to 10^{-2}	4×10^{-2}
$\leqslant 100$	10^{-1} to 1	2
$\leqslant 0.1$		10^{-6} to 2×10^{-5}

Arnoldy, et al.,[89] established a correlation between the integrated x-ray flux with both the 3- and 10-cm integrated radio flux. The x-ray bursts were expressed in terms of absolute energy flux assuming an exponential x-ray spectrum with an e-folding value of 7 keV. In the period from 5 September 1964 to 30 June 1966, there were at least 3 x-ray events with an integrated flux between 0.1 and 1 erg/cm^{-2} in the energy range from 10 to 50 keV.

C. Temporal Variations

There is an enormous variation in the frequency with which solar events occur and in the integrated particle intensity produced. In fact, the eight largest events of solar cycle 19 have produced about 90 percent of all solar cosmic rays above 10 MeV. The annual integrated intensities are shown in Table VII.[65,67] From the limited data available, the following conclusions may be drawn:

(1) Almost the entire integrated intensity for the solar cycle is produced during the six years of maximum activity. The intensity accumulated during sunspot minimum is insignificant.

(2) The annual integrated intensities are lower during sunspot maximum (1957 – 1958) than during the adjacent periods of ascending and particularly descending portions of the solar cycle.

(3) The characteristic rigidity P_O is smaller during sunspot maximum than during the ascending and descending portions of the solar cycle.

Satellite measurements of the integrated intensities of magnetic storm particles >1 MeV are available only since 1961. Their mean characteristic rigidity P_O is 20 MV. The integrated intensities for 1959 and 1960 have been derived from polar glow measurements at 3914Å.[65]

Attempts have been made to correlate the annual integrated intensity of the cosmic ray particles with the number of class 3+ events, the number of major events, and with the monthly smoothed sunspot number averaged over the year. The smoothed sunspot number $\overline{R}_O$ for a given month is defined as[92]

$$\overline{R}_O = (R_{-6} + R_{+6} + 2 \sum_{-5}^{5} R_i)/24 \tag{10}$$

where R_i is the observed monthly Zurich relative sunspot number in months after that month, in which the observed relative number was R_O. The relative sunspot number is defined as

$$R = k(10g + f) \tag{11}$$

where g is the number of sunspot groups, i.e., isolated clusters of sunspots, f is the total number of distinct spots and k is a scale factor depending on the observer. For the relative sunspot numbers observed at Zurich, k = 0.6.

In Fig. 19 the integral solar particle intensity at four different energy levels is plotted as a function of the average annual smoothed sunspot number S over sunspot cycle 19.[65] In years in which S is less than 50, the total number of solar particles above 10 MeV is less than the far more penetrating galactic particle background of $\sim 10^8/cm^2 \cdot$ year.

The integrated proton intensity >1 MeV shows a fair degree of correlation with S. Approximately,

TABLE VII

OBSERVED ANNUAL INTENSITIES OF SOLAR PROTONS

Year	No. of Large Events (Refs. 62, 65, 67, 90)				Average Annual Smoothed Sunspot Number	Integrated Intensity p/cm² (Refs. 65, 67)				P_o (MV)
	Class 3+	Class 3	Others	Total		Magnetic Storm Particles $(E > 1$ MeV$)$	Cosmic Ray Particles $(E > 10$ MeV$)$	$(E > 30$ MeV$)$	$(E > 100$ MeV$)$	
1955		2		2	30		1×10^8			250*
1956	1	1	2	4	120		2.0×10^9	1.0×10^9	3.5×10^8	60
1957	3	2	4	9	182		5×10^9	4.0×10^8	2.0×10^7	50
1958	3	2	3	8	186		7.0×10^9	7.8×10^9	2.4×10^7	70
1959	4	1	1	6	169	1.3×10^{12}†	2.2×10^{10}	4.2×10^9	4.6×10^8	130
1960	6	6	3	15	120	1.8×10^{11}†	6.8×10^9	2.2×10^9	3.8×10^8	90
1961	3	2	1	6	65	8.8×10^{10}	1.6×10^9	3.5×10^8	4.2×10^7	(83)†
1962			2	2	40	3×10^9	8×10^6			
1963	2	1	12	4	28	1×10^{10}	1×10^8	(1.2×10^5)‡	(1×10^4)‡	

* Not in agreement with data in Ref. 67 on p. 86, which states 195.

† From 3914 Å measurements of polar glow (Ref. 91).

‡ Based on event of 23 October 1963 only.

$$\log_{10} I(>1\ MeV) = 9 + 0.02\ S$$

and

$$\log_{10} I(>10\ MeV) = 7 + 0.02\ S \quad . \tag{12}$$

At higher energies there is no correlation. This is not surprising since a single flare may be responsible for the entire annual intensity of the high energy solar protons. Therefore, the correlation appears to be between S and the energetic storm particles rather than the solar protons.

There is also some correlation between the number of events N and S. On the average

$$N = 0.08\ S \quad . \tag{13}$$

An event is here defined as one producing a detectable intensity increase of cosmic rays with energy >10 MeV above the galactic cosmic ray background of 4 particles/cm^2 . sec near earth.[66]

The maximum sunspot number attained in a solar cycle has varied from 45 in cycle 6 to 201.3 in cycle 19. The peak sunspot number in the last four cycles has undergone a systematic increase. Predictions made before the start of cycle 20 and based on the 80-year term variations in the sunspot maxima indicated that cycle 20 will exhibit much lower sunspot numbers than cycle 19.[93-95] More accurate estimates of the magnitude and timing of the sunspot maximum of cycle 20 became possible toward the end of 1967 using Waldmeier's relationship between maximum sunspot number R_M and ascent time t for an even cycle, i.e., the time from minimum to maximum sunspot numbers[96]

$$\log R_M = 2.69 - 0.17\ t \quad . \tag{14}$$

Webber[65] has predicted a maximum sunspot number of 80 to 100 occurring in 1969. Figure 20 shows the smoothed sunspot numbers up to January 1967.[97] The sunspot minima have all been placed at the same point along the time axis. The smoothed sunspot numbers so far observed in cycle 20 indicate that the peak sunspot number will be below that of cycles 18 and 19 and slightly above the mean for cycles 8 through 19. The predicted values shown for cycle 20 have been obtained by a statistical method developed by McNish and Lincoln.[98]

It remains to be shown that the correlation between sunspot number and annual proton intensity >1 MeV and >10 MeV derived during cycle 19 remains valid during the sunspot maximum of cycle 20. Ellison[99] has compared cycles 18 and 19. He found that the frequency of the large flares determining the integrated solar proton intensity did not increase with the sunspot number which was made up mainly by small and medium-sized spot groups. This suggests a rather loose correlation between the sunspot number and the integrated proton intensity. Also, in earlier cycles showing lower sunspot numbers the sunspots were concentrated in larger groups with large penumbral areas.[100] These are likely to produce more intense flare particles.

D. Geomagnetic Cutoff

The earth's geomagnetic field acts as a shield against incoming solar-flare particles of low energies. By applying the Störmer theory for a magnetic dipolar field,[101] Ray and Sauer[102-104] have derived a cutoff rigidity

$$P_c = 14.9/L^2\ GV \tag{15}$$

18

for a point in space defined by McIlwain's magnetic shell parameter L measured in units of earth radii.[16,17] Satellite studies showed that the effective geomagnetic cutoff rigidity of solar cosmic rays are significantly less than the predicted values even during magnetically quiet periods and are further reduced markedly during the main phase of geomagnetic storms.[105-107] Although this effect is variable from event to event, Webber[67] has applied a correction in the form of an average effective value L_{eff} in Eq. (15) from which the average cutoff rigidity may be obtained. Table VIII shows the average cutoff rigidity and cutoff energy E_c of solar protons and alpha particles calculated in this manner for equatorial orbits at $L = 6$ and $L = 6.6$.

TABLE VIII		
AVERAGE GEOMAGNETIC CUTOFF ENERGIES (Ref.67)		
	L = 6.0	L = 6.6
L_{eff}	9.6	10.5
P_c	162 MV	135 MV
E_c	13.9 MeV	9.7 MeV

There is considerable doubt that these cutoff values which have been derived from observations on the ground have any validity in synchronous orbit. In fact it is known that during the peak of a magnetic storm the synchronous orbit may lie outside the earth's magnetic field altogether.

Recent results from the ATS-1 satellite[3,4,11,12] have shown that protons of energy >25 MeV penetrate the synchronous orbit at all times. A variable shielding effect does exist in the energy range from 6 to 20 MeV. There is a diurnal variation with a maximum between 1800 and 0400 local time, showing that proton access is not uniform (see also Ref. 108). It was further observed that protons of solar origin persist for long periods of time in the synchronous orbit, so that during solar maximum interplanetary space is seldom free of them. Recurrent streams of protons are observed near the middle of the 27-day solar rotation cycle.

Figure 21 is a plot of 5-minute count rate averages from LES-4 on 2 September 1966 which shows flare particles penetrating deep into the magnetosphere, where one normally thinks only of stable trapping. The electron channels >150 keV and >850 keV show perfectly normal behavior. At 0648 UT the channel sensitive to protons, 1.8 MeV < E < 50 MeV, starts to rise. An optical flare of importance 3 was observed to start at 0542. The decrease starting at about 0823 is presumably due to the effect of the earth's magnetic field. Thus, in this case both "trapped" particles and particles which have apparently come from the sun occupy the same region of space.

It must be concluded that there exists at present no satisfactory method of calculating average annual intensities of solar protons below 10 MeV in synchronous orbit. Only an upper limit can be given assuming no geomagnetic shielding.

E. Prediction of Solar Flare Intensities in Synchronous Orbit

All predictions on future solar flare particle intensities are based on data obtained during cycle 19, since no meaningful data were available for earlier cycles. Figure 22 shows the integral annual solar proton intensity as a function of rigidity for three cases of interest:

(1) Average intensity for the years 1956 − 1961, covering the years of maximum solar activity of cycle 19.

(2) Intensity for 1959, the highest intensity ever recorded.

(3) Intensity for 1956, which includes the solar flare of 23 February with a characteristic integrated rigidity of 260 MV, the highest rigidity ever recorded.

Many of the predictions of solar cosmic ray intensities are based on a "typical" solar flare presented by Bailey.[109] This hypothetical solar proton event has been constructed from data obtained in the course of six major events during the last sunspot cycle to arrive at a time history for a typical large event. By integrating the flux at different energies over the time of a solar event Keller[110] has obtained the integral and differential energy spectra associated with the "typical flare" shown in Fig. 23. A similar model developed by Lockheed[111] is shown in Fig. 24. The two integral spectra are also shown in Fig. 22 for comparison with the observed annual spectra. It will be noted that Bailey's integrated curve matches the average annual spectrum from 1956 through 1961 very closely both in intensity and in the spectral distribution. The Lockheed spectrum is harder and closer to the 1956 curve.

By using the regression coefficients between annual sunspot number and annual integrated solar particle intensity for cycle 19 [Eq. (12)], and assuming a similar regression curve for cycle 20, Webber[65] arrives at the following values for the worst year of cycle 20:

$$J(>1\,\text{MeV}) \leqslant 10^{11}\,\text{p/cm}^2 \cdot \text{year}$$

$$J(>10\,\text{MeV}) \leqslant 10^{9}\,\text{p/cm}^2 \cdot \text{year} \qquad . \tag{16}$$

These values are an order of magnitude less than the maximum values for cycle 19. As explained in Sec. C, they should apply primarily to energetic storm particles.

The predicted integrated solar flare proton spectrum over the period 1967 − 1973 is shown in Fig. 25. The average curve is based on the assumptions that

(1) $J(>1\,\text{MeV}) = 10^{11}\,\text{p/cm}^2 \cdot \text{year}$.

(2) Characteristic rigidity of the energetic storm particles is the same as that of the 1956 − 1961 average shown in Fig. 15.

(3) The solar flare proton flux above 30 MeV is the same as that of the 1956 − 1961 average.

The average curve is practically identical with a predicted curve by RCA[112] also based on Webber's data.

A maximum predicted curve has been constructed from the limiting conditions:

(1) Characteristics of the energetic storm particles are the same as for the average curve.

(2) The solar flare proton flux between 30 and 100 MeV is the same as that of the 1959 maximum.

(3) At higher energies the flux is the same as that of the 1956 curve, with a characteristic rigidity of 260 MV.

Webber's two predicted points are also shown on the curve. Geomagnetic shielding has not been considered. The alpha particle spectra shown in Fig. 26 have been derived from the corresponding proton spectra by assuming a proton/alpha particle ratio of 2:1 in accordance with the value for an average value of $P_o = 100$ shown in Fig. 10. In the maximum curve, the 1959 spectrum has been continued to energies above 100 MeV, since in the 1956 spectrum the high characteristic

rigidity is coupled to a proton/alpha particle ratio of 50:1. The RCA spectrum, which is based on a proton/alpha particle ratio of 10:1, is also shown.

The predicted integral and differential proton and alpha particle fluxes are listed in Tables IX and X as a function of energy. The average values should be used for long-term applications over periods of several years. The integral fluxes at 9.7 and 13.9 MeV, corresponding to maximum geomagnetic shielding at $L = 6.0$ and $L = 6.6$, are also shown. The minimum shielding thicknesses have been derived from the proton range-energy curves in copper,[56] assuming that alpha particles of the same velocity have the same range.

TABLE IX					
PREDICTED SOLAR FLARE PROTON FLUX OVER THE PERIOD 1967 – 1973					
Energy Range (MeV)		Proton Flux (p/cm^2 · year)				Minimum Shielding to Stop Protons of Energy E_1 (in Cu, Ref. 56) (mg/cm^2)
		Average		Maximum		
E_1	E_2	Integral $(E > E_1)$	Differential $(E_1 < E < E_2)$	Integral $(E > E_1)$	Differential $(E_1 < E < E_2)$	
0.1	0.5	4.2×10^{11}	2.3×10^{11}	4.2×10^{11}	2.3×10^{11}	0.16
0.5	1.0	1.9×10^{11}	9.0×10^{10}	1.9×10^{11}	9.0×10^{10}	1.45
1.0	2.0	1.0×10^{11}	4.4×10^{10}	1.0×10^{11}	4.0×10^{10}	4.5
2.0	3.0	5.6×10^{10}	2.3×10^{10}	6.0×10^{10}	1.7×10^{10}	14.5
3.0	4.0	3.3×10^{10}	1.1×10^{10}	4.3×10^{10}	1.0×10^{10}	28
4.0	5.0	2.2×10^{10}	8.0×10^{9}	3.3×10^{10}	8.0×10^{9}	46
5.0	7.5	1.4×10^{10}	5.6×10^{9}	2.5×10^{10}	8.0×10^{9}	67
7.5	10	8.4×10^{9}	2.7×10^{9}	1.7×10^{10}	4.0×10^{9}	130
9.7	–	6.0×10^{9}	–	1.33×10^{10}	–	200
10	20	5.7×10^{9}	3.3×10^{9}	1.3×10^{9}	6.2×10^{9}	210
13.9	–	3.8×10^{9}	–	1.0×10^{10}	–	370
20	30	2.4×10^{9}	9.0×10^{8}	6.8×10^{9}	2.6×10^{9}	700
30	40	1.5×10^{9}	4.8×10^{8}	4.2×10^{9}	1.6×10^{9}	1,450
40	50	1.02×10^{9}	2.6×10^{8}	2.6×10^{9}	7.8×10^{8}	2,400
50	75	7.6×10^{8}	3.6×10^{8}	1.82×10^{9}	9.4×10^{8}	3,500
75	100	4.0×10^{8}	2.0×10^{8}	8.8×10^{8}	4.2×10^{8}	7,000
100	200	2.0×10^{8}	1.7×10^{8}	4.6×10^{8}	3.4×10^{8}	11,500
200	300	3.1×10^{7}	2.4×10^{7}	1.26×10^{8}	7.0×10^{7}	40,000
300	–	7.0×10^{6}	–	5.6×10^{7}	–	77,000

| TABLE X |
| PREDICTED SOLAR FLARE ALPHA PARTICLE FLUX OVER THE PERIOD 1967 – 1973 |

Energy Range (MeV)		Alpha Particle Flux ($\alpha/cm^2 \cdot$ year)				Minimum Shielding to Stop Alpha Particles of Energy E_1 (mg/cm^2)
		Average		Maximum		
E_1	E_2	Integral ($E > E_1$)	Differential ($E_1 < E < E_2$)	Integral ($E > E_1$)	Differential ($E_1 < E < E_2$)	
1	2	5.0×10^{10}	2.2×10^{10}	5.0×10^{10}	2.0×10^{10}	0.51
2	3	2.8×10^{10}	1.2×10^{10}	3.0×10^{10}	9.0×10^{9}	1.45
3	4	1.6×10^{10}	5.0×10^{9}	2.1×10^{10}	5.0×10^{9}	2.8
4	5	1.1×10^{10}	4.0×10^{9}	1.6×10^{10}	4.0×10^{9}	4.5
5	7.5	7.0×10^{9}	2.8×10^{9}	1.2×10^{10}	3.5×10^{9}	6.75
7.5	10	4.2×10^{9}	1.4×10^{9}	8.5×10^{9}	2.0×10^{9}	13
9.7	–	3.0×10^{9}	–	6.6×10^{9}	–	20
10	20	2.8×10^{9}	1.6×10^{9}	6.5×10^{9}	3.1×10^{9}	21
13.9	–	1.9×10^{9}	–	5.0×10^{9}	–	36
20	30	1.2×10^{9}	4.5×10^{8}	3.4×10^{9}	1.3×10^{9}	67
30	40	7.5×10^{8}	2.4×10^{8}	2.1×10^{9}	8.0×10^{8}	130
40	50	5.1×10^{8}	1.3×10^{8}	1.3×10^{9}	3.9×10^{8}	210
50	75	3.8×10^{8}	1.8×10^{8}	9.1×10^{8}	4.5×10^{8}	310
75	100	2.0×10^{8}	1.0×10^{8}	4.4×10^{8}	2.1×10^{8}	625
100	200	1.0×10^{8}	7.9×10^{7}	2.3×10^{8}	2.0×10^{8}	1,050
200	300	2.1×10^{7}	1.5×10^{7}	2.9×10^{7}	2.3×10^{7}	3,500
300	–	6.0×10^{6}	–	6.3×10^{6}	–	7,000

V. GALACTIC COSMIC RAYS

A. Composition and Spectrum

The particle flux of the galactic cosmic rays is small compared to that of the trapped radiation and of solar flare particles, but will be described here for the sake of completeness. Most of the data on the charge composition and spectra of the various components of the galactic cosmic rays have been taken from Webber's recent comprehensive review.[113] Figure 27 shows the primary spectrum of the total galactic radiation over the rigidity range from 7×10^8 to 10^{18} V.[114,115] At the low rigidity end the intensity increases by about a factor 2 from sunspot maximum to sunspot minimum. Over a wide range the spectrum may be expressed by a power law as a function of energy or rigidity.

$$J(>E) = KE^{\gamma} \quad .$$

Over the entire range 5×10^9 to 5×10^{15} eV

$$J(>E) = 230 \left(\frac{E}{10^{10}}\right)^{-1.60 \pm 0.03}$$

The differential primary spectrum obtained by differentiating the spectrum of Fig. 20 goes through a maximum at 1 GV. At lower energies accurate average data for the primary radiation are difficult to obtain due to uncertainties of the albedo corrections and geomagnetic cutoff and also due to the large effect of the solar modulation. Such data have been obtained recently from satellite measurements, but results over an entire sunspot cycle are not yet available.

The primary galactic cosmic rays are largely composed of protons with helium nuclei next in abundance. On a rigidity basis the proton-helium ratio is ~7.0. The integral proton spectrum may be obtained directly from Fig. 27 by decreasing the ordinate by the 18 percent contribution of the heavier nuclei. The more recent balloon measurements with Cerenkov-scintillation counters[116] shown in Fig. 28 exhibit somewhat higher proton intensities. In the rigidity range from 3 to 20 GV the proton spectrum may be expressed as

$$J(>P) = 7000 \, P^{-1.5} \, p/m^2 \cdot sr \cdot sec \quad ,$$

where P is in gigavolts. The differential proton spectrum at low rigidities has been obtained by Webber[113] from observations in 1963. It is shown in Fig. 29 together with the results of balloon and satellite measurements carried out at sunspot minimum by Balasubrahmanyan[117] and electron measurements by L'Heureux and Meyer.[118] The proton spectrum has a few peaks at about 1 GV and falls off sharply at lower rigidities.

The integral helium spectrum shown in Figs. 27 and 28 is similar to the proton spectrum and may be given the form

$$J(>P) = 900 \, P^{-1.5} \, \text{helium nuclei}/m^2 \cdot sr \cdot sec$$

over the rigidity range from 5 to 20 GV. The differential helium spectrum peaks at 1.35 GV. Between 2.5 and 12 GV the differential rigidity spectra of helium and all heavier nuclei may be represented by power laws with exponent -2.2. At higher rigidities the exponent increases to -2.5 or -2.6 above 100 GV.[119] The abundance of the heavier nuclei is listed in Table V, Sec. IV. Their integral spectra are similar to those of the protons and of helium, their differential spectra peak at somewhat higher rigidities. The d/p ratio is less than 6 percent in the energy range

TABLE XI

INTEGRAL FLUX OF GALACTIC COSMIC RAYS AT SUNSPOT MINIMUM

Energy (GeV)	Protons		He-Nuclei		Electrons	
	Flux (protons/cm^2 · year) (Ref. 116)	Minimum Shielding (g/cm^2) (in Cu, Ref. 124)	Flux (He nuclei/cm^2 · year) (Ref. 116)	Minimum Shielding (g/cm^2) (based on p range in Cu, Ref. 124)	Flux (e/cm^2 · year) (Ref. 120)	Minimum Shielding (g/cm^2) (in Pb, Ref. 125)
0.1	1.5×10^8	11.8	1.5×10^7	1.05	5.2×10^6	20
0.5	1.2×10^8	172	1.4×10^7	17.3	2.5×10^6	28
1.0	8.3×10^7	472	1.2×10^7	56.6	1.2×10^6	30
5.0	1.9×10^7	3165	3.9×10^6	630	3.2×10^5	36
10	7.5×10^6	6258	2.1×10^6	1493	1.6×10^5	39
20	3.1×10^6	–	9.1×10^5	3165	8.0×10^4	42

$25 - 80$ MeV/nucleon; about 30 to 40 percent of the helium nuclei consist of He[3] on a rigidity basis.[114] The present state of knowledge on primary cosmic ray electrons and positrons has been summarized by Meyer[115] and Waddington.[114] Between 500 MeV and 3.5 GeV, L'Heureux and Meyer[118] obtained a differential spectrum of the form

$$\frac{dJ}{dE} = 11 \times E^{-1.6} e/m^2 \cdot sec \cdot sr \cdot GeV$$

and by inference an integral spectrum with exponent -0.6. An extrapolation of this spectrum to lower energies is in agreement with previous experimental results. Webber and Chotkowski[120] obtained a differential spectrum

$$\frac{dJ}{dE} = 30 \times E^{-1.8} e/m^2 \cdot sec \cdot sr \cdot GeV \quad .$$

Between 16 and 50 GeV, Daniel and Stephens[121] obtained an integral spectrum exponent -1.16. About 30 to 40 percent of the particles are positrons. The fraction of positrons seems to decrease with energy.

Gould and Burbidge[122] have reviewed the experimental measurements on high energy photons from cosmic sources. Figure 30 shows the spectrum of the isotropic cosmic background photon fluxes extrapolated from a few observations at different energies. Figure 31 shows the differential spectrum taken from the paper by Rocchia, et al.[123] In addition discrete galactic x-ray sources produce fluxes on the order of 10^{-8} to 10^{-7} ergs/cm$^2 \cdot$ sec.

The integral flux of galactic protons, helium nuclei and electrons at sunspot minimum is shown in Table XI for different energies. The radiation is very low in intensity but very penetrating.

B. Temporal Variations

The galactic cosmic radiation is modulated by the sun resulting in three major classes of time variations[126,127]

(1) Solar Cycle Variations:— The intensity varies in anticorrelation with the sunspot activity lagging by about 9 months during increasing solar activity and by 18 months during periods of decreasing solar activity. The modulation is a function of rigidity and takes the form $\exp(-K/P)$ in the rigidity range $0.5 < P < 50$ GV.[128] At 1 GV the cosmic ray intensity increases by a factor 2 from sunspot maximum to sunspot minimum.

(2) Forbush Decreases:— Forbush decreases in the cosmic ray intensity on the order of 20 percent >1 GV usually occur in association with magnetic storms and last from 2 days to 2 weeks. Small decreases are correlated to the 27-day cycle of magnetic activity.

(3) Local Time Variations:— Very small diurnal variations (<0.5 percent >1 GV) take place in the cosmic ray intensity with an average maximum between 1300 and 1500 hours.

C. Geomagnetic Cutoff

The geomagnetic cutoff rigidity P_c defined in Eq. (15), Sec. IV, is a more meaningful parameter for galactic cosmic rays during sunspot minimum than for solar particles. Equation (15) would indicate a cutoff rigidity of 340 MV or a cutoff energy of 60 MeV at $L = 6.6$. This is below the peak energy of the primary radiation, so that almost the entire primary cosmic ray intensity will reach the equatorial synchronous orbit. Even under these conditions the cutoff rigidity is subject to the following uncertainties:

TABLE XII		
CHARGED PARTICLE RADIATION		
Particles	Energy Range	Total Dose per Year in Equatorial Synchronous Orbit (particles/cm^2)
Trapped Electrons	<5 eV	10^{17}
	>200 eV	10^{17}
	>10 keV	2.1×10^{15}
	>100 keV	1.1×10^{15}
	>1 MeV	1.5×10^{13}
Trapped Protons	<5 eV	10^{17}
	>200 eV	10^{17}
	>1.8 keV	6×10^{15}
	>100 keV	3.8×10^{14}
	>1 MeV	5.4×10^{10}
Solar Protons (maximum)	>1 MeV	1×10^{11}
	>10 MeV	1.3×10^{10}
	>100 MeV	4.6×10^{8}
Solar Alpha Particles (maximum)	>1 MeV	5×10^{10}
	>10 MeV	6.5×10^{9}
	>100 MeV	2.3×10^{8}
Galactic Cosmic Rays (maximum)	>100 MeV	1.7×10^{8}

TABLE XIII		
EFFECT OF SHIELDING ON CHARGED PARTICLE RADIATION IN EQUATORIAL SYNCHRONOUS ORBIT		
	Total Dose per Year* (particles/cm^2)	
	6-mil SiO$_2$	7-mil Kovar
Electrons	3.9×10^{14}	1.3×10^{14}
Protons	2×10^{10}	8×10^{9}
Alpha Particles	2.5×10^{9}	1×10^{9}
*Omnidirectional flux with infinite shielding over 2π steradians.		

(1) No experimental determinations of the cutoff rigidity in synchronous orbit have been published. L = 6.6 may not be a good parameter.

(2) The geomagnetic cutoff is not sharp.[129]

(3) At low altitudes Eq. (15) should be replaced by[130]

$$P_c = KL^\gamma$$

where K varies from 15.02 to 16.69 and γ is close to -2.

VI. SUMMARY

Table XII summarizes the charged particle radiation in the equatorial synchronous orbit. It may be noted that there are large doses of very low energy radiation requiring only minimal shielding, whereas the more penetrating radiation is far less intense. While it is beyond the scope of this report to consider the effect of different shielding configurations on the incident charged particle spectra (see Refs. 131, 132), two situations are of special interest to communication satellites in synchronous orbit:

(a) 6-mil SiO_2, the minimum shielding applied to the silicon solar cells.

(b) 7-mil Kovar or nickel, the minimum shielding provided by the can or cover of a hermetically sealed simiconductor device.

Table XIII indicates that even these two minimum shielding conditions remove all charged particles except trapped electrons as well as some solar flare protons and alpha particles. Additional shielding information is provided in the tables in the text. It should be noted that the shielding itself creates bremsstrahlung which may contribute a significant amount of ionizing radiation when most of the primary radiation has been cut off.

REFERENCES

1. Applications Technology Satellite Technical Data Report, Sec. 11, "Environmental Measurements Experiments" (March 1968).

2. G. A. Paulikas, et al., "First Quarterly Report for ATS-1 Omnidirectional Spectrometer," Technical Data Report for the Applications Technology Satellite (ATS) Program, Goddard Spaceflight Center, Greenbelt, Md. (1967).

3. _____, "Second Quarterly Report for ATS-1 Omnidirectional Spectrometer," Technical Data Report for the Applications Technology Satellite (ATS) Program, Goddard Spaceflight Center, Greenbelt, Md. (1967).

4. _____, "Third Quarterly Report for ATS-1 Omnidirectional Spectrometer," Technical Data Report for the Applications Technology Satellite (ATS) Program, Goddard Spaceflight Center, Greenbelt, Md. (1967).

5. _____, "Final Quarterly Report for ATS-1 Omnidirectional Spectrometer," Technical Data Report for the Applications Technology Satellite (ATS) Program, Goddard Spaceflight Center, Greenbelt, Md. (1968).

6. T. W. Lezniak, et al., "Conjugate Effects on Energetic Electrons Between the Equator at 6.6 R_e and the Auroral Zone," Applications Technology Satellite Technical Data Report, Sec. 11.4 A, Appendix A, Part 1 (March 1968) and Technical Report CR-103, University of Minnesota (1967).

7. J. W. Freeman and J. J. Maguire, "On the Variety of Particle Phenomena Discernible at the Geostationary Orbit via the ATS-1 Satellite" to be published in Ann. Géophys.

8. J. W. Freeman and D. T. Young, "Highly Directional Fluxes of Low-Energy Ions at the Synchronous Altitude, 1. The Observations," Trans. Am. Geophys. Un. 49, No. 1, 227-228 (1968).

9. T. W. Lezniak and J. R. Winckler, "Evidence for a Physical Motion of the Magnetospheric Boundary Associated with the Magnetospheric Substorm," Trans. Am. Geophys. Un. 49, No. 1, 229 (1968).

10. G. K. Parks, et al., "The Magnetospheric Substorm: The Fundamental Mode of Production of Energetic Trapped Electrons in the Magnetosphere," Trans. Am. Geophys. Un. 49, No. 1, 228-229 (1968).

11. C. S. Roberts, et al., "Synchronous Altitude Observation of Energetic Protons During the Solar Proton Event of 28 January 1967," Trans. Am. Geophys. Un. 49, No. 1, 275-276 (1968).

12. J. B. Blake, et al., "Observations of Solar Protons at Synchronous Altitude," Trans. Am. Geophys. Un. 49, No. 1, 276 (1968).

13. L. J. Lanzerotti, et al., "Temporal Variations in the Electron Flux at Synchronous Altitudes," J. Geophys. Res. 72, No. 23, 5893-5902 (1 December 1967).

14. J. I. Vette, et al., "Models of the Trapped Radiation Environment, Vol. II: Inner and Outer Zone Electrons," NASA SP-3024 (1966).

15. J. I. Vette and A. B. Lucero, "Models of the Trapped Radiation Environment, Vol. III: Electrons at Synchronous Altitudes," NASA SP-3024 (1967).

16. C. E. McIlwain, "Coordinates for Mapping the Distribution of Magnetically Trapped Particles," J. Geophys. Res. 66, No. 11, 3681-3691 (November 1961).

17. _____, "Magnetic Coordinates" in Radiation Trapped in the Earth's Magnetic Field, Ed. B. M. McCormac (Reidel, Holland, 1966), pp. 45-61.

18. R. D. Evans, The Atomic Nucleus (McGraw-Hill, New York, 1955).

19. W. D. Brown, "ATS Power Subsystem Radiation Effects Study, Phase 1/Final Report," Appendix A, "Synchronous Orbit Radiation Environment," Hughes Aircraft Company, SSD 80089R, NASA Contract NAS 5-3823, February 1968.

20. J. O'Brien, "A Large Diurnal Variation of the Geomagnetically Trapped Radiation," J. Geophys. Res. 68, No. 4, 989-995 (15 February 1963).

21. G. D. Mead, "The Motion of Trapped Particles in a Distorted Field" in Radiation Trapped in the Earth's Magnetic Field, Ed. B. M. McCormac (Reidel, Holland, 1966), pp. 481-490.

22. W. D. Brown, "Synchronous Orbit Trapped Radiation Environment," Technical Memorandum SSD 60252R, Report No. 8, Hughes Aircraft Company, Space Systems Division (June 1966).

23. K. A. Pfitzer and J. R. Winckler, "Energy Spectra of Electrons in the Radiation Belts from 50 keV to 4 MeV," Trans. Am. Geophys. Un. 46, No. 124 (1965).

24. _____, "Time and Space Variations of Electrons in the Inner and Outer Zones During the Fall of 1964 and 1965," Trans. Am. Geophys. Un. 47, No. 130 (1966).

25. K. A. Pfitzer, et al., "The Spectra and Intensity of Electrons in the Radiation Belts," Space Research III, pp. 702-713 (1966).

26. S. R. Kane, et al., "Latitude and Local Time Dependence of Iso-Intensity Contours for Electrons with Energies Greater than 700 keV in the Outer Radiation Zone," Trans. Am. Geophys. Un. 47, No. 134 (1966).

27. W. N. Hess, et al., "Advances in Particles and Field Research in the Satellite Era," Rev. Geophys. 3, No. 4, 521-570 (November 1965).

28. J. W. Freeman and J. J. Maguire, "Gross Local-Time Particle Asymmetries at the Synchronous Orbit Altitude," J. Geophys. Res. 72, No. 21, 5257-5264 (1 November 1967).

29. L. A. Frank, "On the Local-Time Dependence of Outer Radiation Zone Electron (E > 1.6 MeV) Intensities near the Magnetic Equator," J. Geophys. Res. 70, No. 17, 4131-4138 (1 September 1965).

30. _____, "A Survey of Electrons E > 40 keV Beyond 5 Earth Radii with Explorer 14," J. Geophys. Res. 70, No. 7, 1593-1626 (1 April 1965).

31. R. P. Lin and K. A. Anderson, "Periodic Modulations of the Energetic Electron Fluxes in the Distant Radiation Zone," J. Geophys. Res. 71, No. 7, 1827-1835 (1 April 1966).

32. C. E. McIlwain, "Processes Acting Upon Outer Zone Electrons. I. Adiabatic Perturbations," SP-66-5 University of California, San Diego (1966).

33. D. J. Williams, " A 27-Day Periodicity in Outer Zone Trapped Electron Intensities," J. Geophys. Res. 71, No. 7, 1815-1826 (1 April 1966).

34. B. J. O'Brien, "The Trapped-Radiation Zones," in Space Physics, Eds. D. P. LeGalley and A. Rosen (Wiley, New York, 1964).

35. L. A. Frank and J. A. Van Allen, "Correlation of Outer Radiation Zone Electrons (E_e ~ 1 MeV) with the Solar Activity Cycle," J. Geophys. Res. 71, No. 11, 2697-2700 (1 June 1966).

36. T. A. Farley and N. L. Sanders, "Pitch Angle Distributions and Mirror Point Densities in the Outer Radiation Zone," J. Geophys. Res. 67, No. 6, 2159-2168 (June 1962).

37. L. A. Frank, "On the Extraterrestrial Ring Current During Geomagnetic Storms," J. Geophys. Res. 72, No. 15, 3753-3767 (1 August 1967).

38. _____, "Initial Observations of Low-Energy Electrons in the Earth's Magnetosphere with OGO 3," J. Geophys. Res. 72, No. 1, 185-195 (1 January 1967).

39. _____, "Several Observations of Low-Energy Protons and Electrons in the Earth's Magnetosphere with OGO 3," J. Geophys. Res. 72, No. 7, 1905-1916 (1 April 1967).

40. J. W. Freeman, et al., "Explorer 12 Observations of the Magnetospheric Boundary and the Associated Solar Plasma on September 13, 1961," J. Geophys. Res. 68, No. 8, 2121-2130 (15 April 1963).

41. J. W. Freeman, "The Morphology of the Electron Distribution in the Outer Radiation Zone and Near the Magnetospheric Boundary as Observed by Explorer 12," J. Geophys. Res. 67, No. 9, 1691-1723 (1 May 1964).

42. V. V. Bezrukikh, et al., "Preliminary Results of Measurements Carried Out by Means of Charged Particle Traps on the Interplanetary Station Zond 2," Space Science VI, 862-869 (1966).

43. K. I. Gringauz, et al., "Measurements Made in the Earth's Magnetosphere by Means of Charged Particle Traps Aboard the MARS 1 Probe," Space Research IV, 621-626 (1964).

44. G. P. Serbu and E. J. R. Maier, "Low Energy Electrons Measured on IMP 2," J. Geophys. Res. 71, No. 15, 3755-3766 (1 August 1966).

45. G. P. Serbu, "Results from the IMP-1 Retarding Potential Analyzer," Space Research $\underline{V}$, 564-574 (1965).

46. _____ and E. J. R. Maier, "Thermal Plasma Measurements Within the Magneto-sphere," Space Research $\underline{VII}$, 527-534 (1967).

47. V. I. Slysh, "The Measurement of Cosmic Radio Emission at 210 and 2200 Kilocycles per Second to Eight Earth Radii on the Automatic Interplanetary Station Zond-2," Cosmic Research $\underline{3}$, 760-767 (September – October 1965).

48. J. A. Van Allen and S. M. Krimigis, "Trapped Alpha Particles in the Earth's Outer Radiation Zone," Trans. Am. Geophys. Un. $\underline{46}$, 140 (1965).

49. S. M. Krimigis and J. A. Van Allen, "Geomagnetically Trapped Alpha Particles," J. Geophys. Res. $\underline{72}$, No. 23, 5779-5797 (1 December 1967).

50. L. R. Davis and J. M. Williamson, "Low Energy Trapped Protons," Space Research $\underline{III}$, 365-375 (1963).

51. L. R. Davis, "Low Energy Trapped Protons and Electrons," in Proceedings of the Plasma Space Science Symposium, Eds. C.C. Chang and S.S. Huang (Reidel, Holland, 1965).

52. _____ and J. M. Williamson, "Outer Zone Protons," in Radiation Trapped in the Earth's Magnetic Field, Ed. B. M. McCormac (Reidel, Holland, 1966), pp. 215-229.

53. S. N. Vernov, et al., "Measurements of Low-Energy Protons from Cosmos-41 Satellite," Space Research $\underline{VI}$, 734-745 (1966).

54. S. M. Krimigis and T. P. Armstrong, "Observations of Protons in the Magnetosphere with Mariner 4," J. Geophys. Res. $\underline{71}$, No. 19, 4641-4650 (October 1966).

55. J. H. King, "Models of the Trapped Radiation Environment, Vol. IV: Low Energy Protons," NASA SP-3024, Washington, D. C. (1967).

56. H. A. Bethe and J. Ashkin, "Passage of Radiations Through Matter," in Experimental Nuclear Physics, Vol. 1, Ed. E. Segrè (Wiley, New York, 1953).

57. H. A. Taylor, et al., "Positive Ion Composition in the Magnetoionosphere Obtained from the OGO-A Satellite," J. Geophys. Res. $\underline{70}$, No. 23, 5769-5781 (1 December 1965).

58. F. N. Byrne, et al., "A Survey of Solar Flare Phenomena," Space Sci. Rev. $\underline{3}$, 319-341 (1964).

59. W. R. Webber, "Time Variations of Low Rigidity Cosmic Rays During the Recent Sunspot Cycle," Progress in Elementary Particle and Cosmic Ray Physics, Vol. VI, Eds. J. G. Wilson and S. A. Wouthuysen (North-Holland Publishing Co., 1962), pp. 75-243.

60. G. Godoli and C. W. Allen, "The Indices of Solar Activity," Planet. Space Sci. $\underline{12}$, 349-354 (1964).

61. S. Biswas and C. E. Fichtel, "Composition of Solar Cosmic Rays," Space Sci. Rev. $\underline{4}$, 709-736 (September 1965).

62. F. B. McDonald, "Solar Proton Manual," NASA Technical Report TR R-169 (September 1963).

63. P. S. Freier and W. R. Webber, "Exponential Rigidity Spectrums for Solar-Flare Cosmic Rays," J. Geophys. Res. $\underline{68}$, No. 6, 1605-1629 (15 March 1963).

64. A. Rosen, "The Dynamics of the Outer Radiation Zone," Space Science, Ed. D. P. LeGalley (Wiley, New York, 1963), pp. 275-315.

65. W. R. Webber, "An Evaluation of Solar-Cosmic-Ray Events During Solar Minimum," Boeing Co. Technical Report D2-84274-1 (June 1966).

66. _____, "A Review of Solar Cosmic Ray Events," AAS-NASA Symposium on the Physics of Solar Flares, NASA SP-50, Ed. W. N. Hess, 215-255 (1964).

67. _____, "An Evaluation of the Radiation Hazard Due to Solar Particle Events," Boeing Co. Report No. D2-90469 (December 1963).

68. _____, "Solar-Flare Proton Data," Nucleonics $\underline{21}$, 154-157 (August 1963).

69. J. L. Modisette, et al., "Model Solar Proton Environments for Manned Spacecraft Design," TN D-2746, NASA Technical Note (April 1965).

70. K. Sakurai, "On the Nuclear Abundance and Rigidity Spectra of Solar Cosmic Rays," Planet. Space Sci. $\underline{13}$, No. 8, 867-868 (1965).

71. M. V. K. Apparao, et al., "Fast Neutrons of Solar Origin," Proceedings of the International Conference on Cosmic Rays, London, Vol. 1 (September 1965), pp. 358-361.

72. D. A. Bryant, et al., "New Evidence for Long-Lived Solar Streams in Interplanetary Space," Phys. Rev. Letters 11, No. 4, 144-146 (15 August 1963).

73. J. Bartels, "Terrestrial-Magnetic Activity and Its Relation to Solar Phenomena," Terr. Mag. Atm. Elect. 37, 1-52 (March 1932).

74. _____, "Twenty-Seven Day Recurrences in Terrestrial Magnetic and Solar Activity, 1923 – 1933," Terr. Mag. Atm. Elect. 39, 201 – 202 (1934).

75. C. W. Allen, "M-Regions," Planet. Space Science 12, 487-494 (1964).

76. C. W. Snyder and M. Neugebauer, "Interplanetary Solar-Wind Measurements by Mariner II," Space Res. 4, 89-113 (1964).

77. G. Comstock, et al., "Composition and Spectra of Charged Particles of Solar and Cosmic Origin Measured on Satellites," in Recent Advances in Cosmic Ray Research, Eds. J. Gauger and A. J. Masley (Western Periodicals Company, No. Hollywood, California) (1966).

78. R. P. Lin and K. A. Anderson, "Electrons >40 keV and Protons >500 keV of Solar Origin," Solar Phys. 1, 446-464 (1967).

79. C. DeJager, "Solar X Radiation," Ann. Astrophys. 28, 125-131 (1965).

80. G. G. Fazio and E. M. Hafner, "The OSO 1 High-Energy Gamma-Ray Experiment," J. Geophys. Res. 72, No. 9, 2452-2455 (1 May 1967).

81. L. E. Peterson and J. R. Winckler, "Gamma-Ray Burst from a Solar Flare," J. Geophys. Res. 64, No. 7, 697-707 (July 1959).

82. T. A. Chubb, et al., "X-Ray Emission Accompanying Solar Flares and Non-Flare Sunspot Maximum Conditions," Space Res. 1, 695-701 (1960).

83. _____, "Measurements Made of High-Energy X-Rays Accompanying Three Class 2+ Solar Flares," J. Geophys. Res. 65, No. 5, 1331-1332 (June 1960).

84. J. R. Winckler, et al., "Observations of a Solar Bremsstrahlung Burst of 1926 UT, August 11, 1960," J. Geophys. Res. 66, No. 1, 316-320 (January 1961).

85. J. I. Vette and F. G. Casal, "High-Energy X-Rays During Solar Flares," Phys. Rev. Letters 6, 334-336 (1 April 1961).

86. K. A. Anderson and J. R. Winckler, "Solar Flare X-Ray Burst on September 1961," J. Geophys. Res. 67, No. 11, 4103-4117 (October 1962).

87. S. L. Mandelstam, "X-Ray Emission of the Sun," Space Sci. Rev. 4, 587-665 (1965).

88. H. H. Malitson, "The Solar Energy Spectrum," Sky and Tel. 29, 162-165 (1965).

89. R. L. Arnoldy, et al., "A Study of Energetic Solar Flare X-Rays," Solar Phys. 2, 171-178 (September 1967).

90. A. J. Masley and A. D. Goedeke, "Solar Cosmic Ray Event Characteristics, Solar Minimum Versus Solar Maximum," Space Res. VII, 797-804 (1967).

91. B. P. Sandford, "Polar-Glow Aurora in Polar Cap Absorption Events," J. Atmos. Terr. Phys. 24, 155 (1962).

92. M. Waldmeier, The Sunspot Activity in the Years 1610-1960 (Schulthes, Zurich, 1961).

93. C. M. Minnis, "An Estimate of the Peak Sunspot Number in 1968," Nature 186, 462 (7 May 1960).

94. W. Gleissberg, "Der Charakter des nächsten Sonnenfleckenmaximum," Z. Astrophys. 49, 25-29 (1960).

95. B. M. Rubashev, "Problems of Solar Activity," NASA Technical Translation, NASA TT F-244 (December 1964).

96. M. Waldmeier, "Neue Eigenschaften der Sonnenfleckenkurve," Astronomische Mitteilungen, Sternwarte der Eidgen. Technischen Hochschule in Zürich, 133, 106-129 (1935).

97. Solar-Geophysical Data, No. 278, Institutes of Environmental Research, U. S. Department of Commerce, Environmental Science Service Administration (October 1967).

98. A. G. McNish and J. V. Lincoln, "Prediction of Sunspot Numbers," Trans. Am. Geophys. Un. 30, 673-685 (October 1949).

99. M. A. Ellison, "Recent Solar Activity," Nature 4596, 1173 (30 November 1957).

100. K. A. Anderson, "Energetic Solar Particles," in Space Physics, Eds. D. P. LeGalley and A. Rosen (Wiley, New York, 1964).

101. C. Störmer, Polar Aurora (Oxford University Press, London, 1955).

102. E. C. Ray, "On the Motion of Charged Particles in the Geomagnetic Field," Ann. Phys. 24, 1-18 (October 1963).

103. H. H. Sauer and E. C. Ray, "On Cosmic Ray Cut-Offs," Ann. Phys. 25, 135-142 (1963).

104. H. H. Sauer, "A New Method of Computing Cosmic-Ray Cut-Off Rigidity for Several Geomagnetic Field Models," J. Geophys. Res. 68, No. 4, 957-971 (15 February 1963).

105. S. I. Akasofu, et al., "The Anomalous Entry of Low-Rigidity Solar Cosmic Rays into the Geomagnetic Field," J. Geophys. Res. 68, No. 19, 5327-5338 (1963).

106. I. G. F. Pieper, et al., "Solar Proton and Magnetic Storms in July 1961," J. Geophys. Res. 67, No. 13, 4959-4981 (1962).

107. W. R. Webber, "The Motion of Low-Rigidity Cosmic Rays in the Earth's Magnetic Field and the Effects of External Fields," J. Geophys. Res. 68, No. 10, 3065-3085 (15 May 1963).

108. G. A. Paulikas, et al., "Low-Energy Solar-Cosmic-Ray Cutoffs: Diurnal Variations and Pitch Angle Distributions," J. Geophys. Res. 73, No. 1, 87-95 (1 January 1968).

109. D. K. Bailey, "Time Variations of the Energy Spectrum of Solar Cosmic Rays in Relation to the Radiation Hazard in Space," J. Geophys. Res. 67, No. 1, 391-396 (January 1962).

110. J. W. Keller, "Large Range NASA Shielding Requirements," Proceedings of the Symposium on the Protection Against Radiation in Space, Gatlinburg, Tennessee, 5-7 November 1962, pp. 662-681.

111. Study of a Rotating Manned Orbital Space Station, Final Report, Vol. II, Section 3, LR 17502, Spacecraft Organization, Lockheed-California, Burbank, California (March 1964).

112. "Space Environment," Manned Mission Photovoltaic Power Systems Study, Vol. III, Supporting Documentation, Appendix E, Final Report, AED-R-3155 by RCA Astro-Electronics Division for Propulsion and Power Division, NASA Manned Spacecraft Center, Houston, Texas under Contract NAS 9-5266, 9 June 1967.

113. W. R. Webber, "The Spectrum and Charge Composition of the Primary Cosmic Radiation," Handbuch der Physik, 46/2, Cosmic Rays, Vol. II, Ed. K. Sitte (Springer, Berlin, 1967), pp. 181-264.

114. C. J. Waddington, "Spectral Composition," Proceedings of the International Conference on Cosmic Rays, London, Vol. 1 (September 1965), pp. 462-468.

115. P. Meyer, "Primary Electrons and Positrons in the Cosmic Radiation," Proceedings of the International Conference on Cosmic Rays, London, Vol. 1 (September 1965), pp. 61-67.

116. J. F. Ormes and W. R. Webber, "Measurements of the Primary Proton and Helium Spectra and Their Modulations Using a Balloon-Borne Cerenkov-Scintillation Counter," Proceedings of the International Conference on Cosmic Rays, London, Vol. 1 (September 1965), pp. 349-354.

117. V. K. Balasubrahmanyan, et al., "Galactic Cosmic Rays at Solar Minimum, 1965," Proceedings of the International Conference on Cosmic Rays, London, Vol. 1 (September 1965), pp. 427-436.

118. J. L'Heureux and P. Meyer, "The Flux and Energy Spectrum of Primary Cosmic Ray Electrons," Phys. Rev. Letters 15, 93 (1965).

119. W. R. Webber and J. F. Ormes, "Cerenkov-Scintillation Counter Measurements of Nuclei Heavier Than Helium in the Primary Cosmic Radiation," J. Geophys. Res. 72, No. 23, 5957-5976 (1 December 1967).

120. W. R. Webber and C. Chotkowski, "A Determination of the Energy Spectrum of Extraterrestrial Electrons in the Energy Range 70-2000 MeV," J. Geophys. Res. 72, No. 11, 2783-2802 (1 June 1967).

121. R. R. Daniel and S. A. Stephens, "The Electron Component of the Primary Cosmic Radiation at Energies ≥ 15 GeV," Proceedings of the International Conference on Cosmic Rays, London, Vol. I (September 1965), pp. 335–338.

122. R. J. Gould and G. R. Burbidge, "High Energy Photons and Neutrinos from Cosmic Sources," Handbuch der Physik, 46/2, Cosmic Rays, Vol. II, Ed. K. Sitte (Springer, Berlin, 1967) pp. 265–309.

123. R. Rocchia, et al., "Flux and Energy Spectra of Primary Cosmic X and Gamma-Rays Between 20 keV and 1 MeV," Space Res. VII, 1327–1333 (1967).

124. M. Rich and R. Madey, "Range-Energy Tables," Radiation Laboratory, University of California UCRL-2301 (March 1954).

125. W. Heitler, The Quantum Theory of Radiation, 3rd ed. (Clarendon Press, Oxford, 1954).

126. S. E. Forbush, "Time-Variations of Cosmic Rays," Handbuch der Physik, 49/1, Geophysics, Vol. III, Part 1, Ed. J. Bartels (Springer, Berlin, 1966), pp. 159–247.

127. J. Quenby, "The Time Variations of the Cosmic Ray Intensity," Handbuch der Physik, 46/2, Cosmic Rays, Vol. II, Ed. K. Sitte (Springer, Berlin, 1967), pp. 310–371.

128. J. A. Lockwood and W. R. Webber, "The 11-Year Solar Modulation of Cosmic Rays as Deduced from Neutron Monitor Variations and Direct Measurements at Low Energies," J. Geophys. Res. 72, No. 23, 5977–5989 (1 December 1967).

129. W. R. Webber and F. B. McDonald, "Cerenkov Scintillation Counter Measurements of the Intensity and Modulation of Low Rigidity Cosmic Rays and Features of the Geomagnetic Cutoff Rigidity," J. Geophys. Res. 69, No. 15, 3097–3114 (1 August 1964).

130. D. F. Smart and M. A. Shea, "A Study of the Effectiveness of the McIlwain Coordinates in Estimating Cosmic-Ray Vertical Cut-Off Rigidities," J. Geophys. Res. 72, No. 13, 3447–3454 (1 July 1967).

131. C. L. Mack, "Van Allen Belt Simulation," AIAA Paper No. 67-177, AIAA Fifth Aerospace Sciences Meeting, New York (23-26 January 1967).

132. C. L. Mack, "The Internal Radiation Environment of Cylindrical Spacecraft," IEEE Trans. Nuclear Sci. NS-14, 204–209 (December 1967).
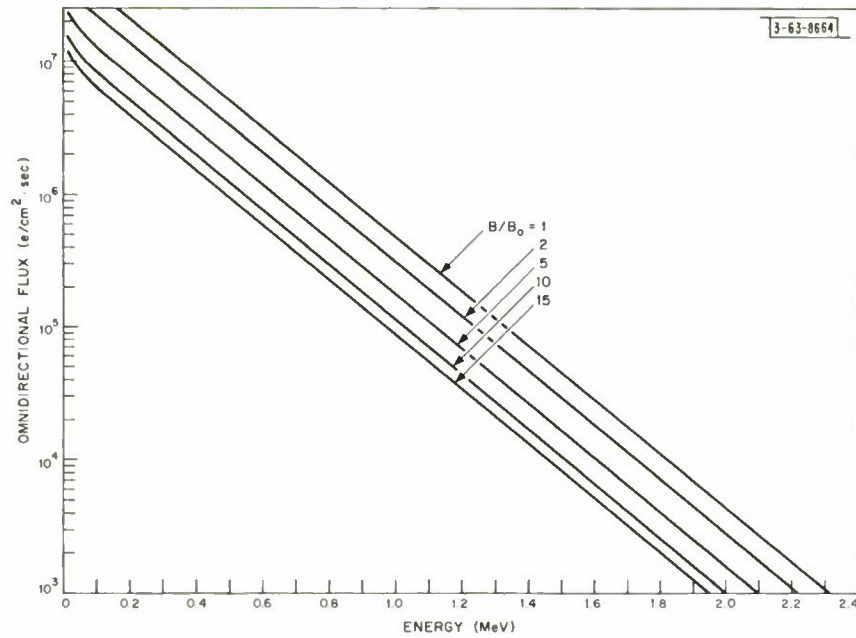
Fig. 1.   Integral spectrum of trapped electrons in synchronous orbit averaged over local time (taken from J. I. Vette and A. B. Lucero, Ref. 15).
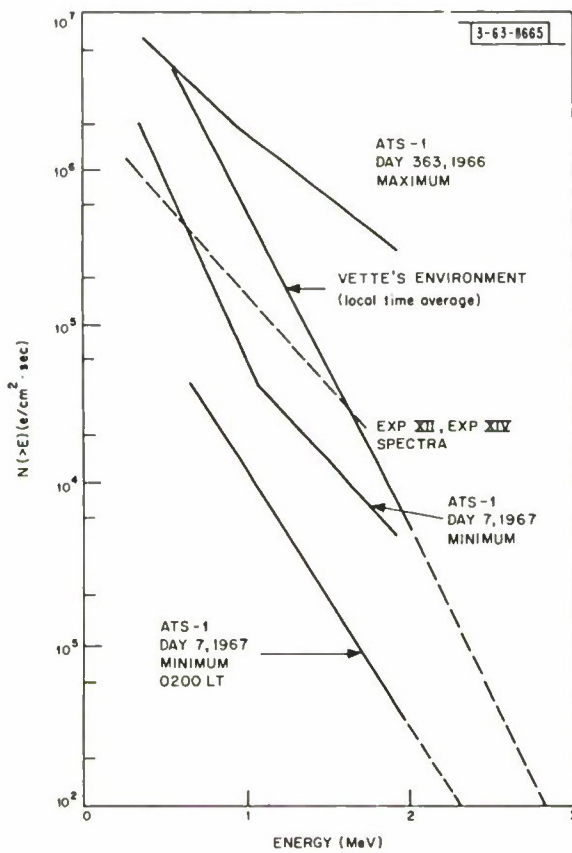
Fig. 2.   Comparison of energy spectra of trapped electrons in synchronous orbit (taken from W. D. Brown, Ref. 19).

Fig. 3. LES-4 electron spectra.
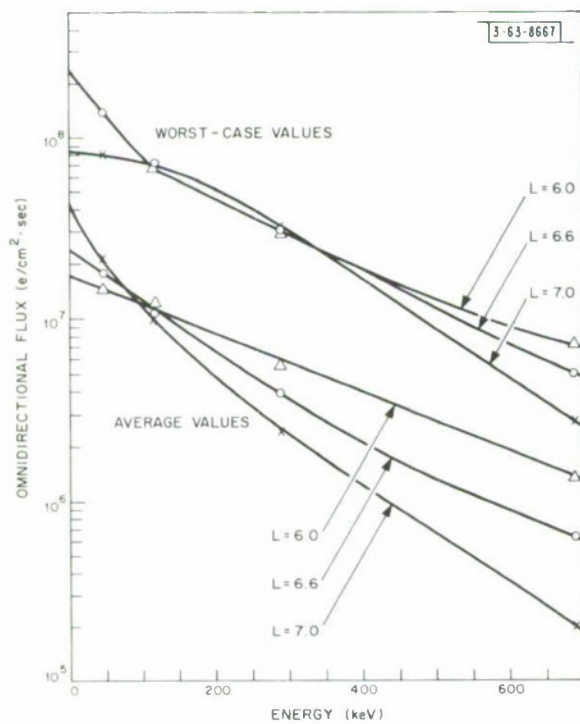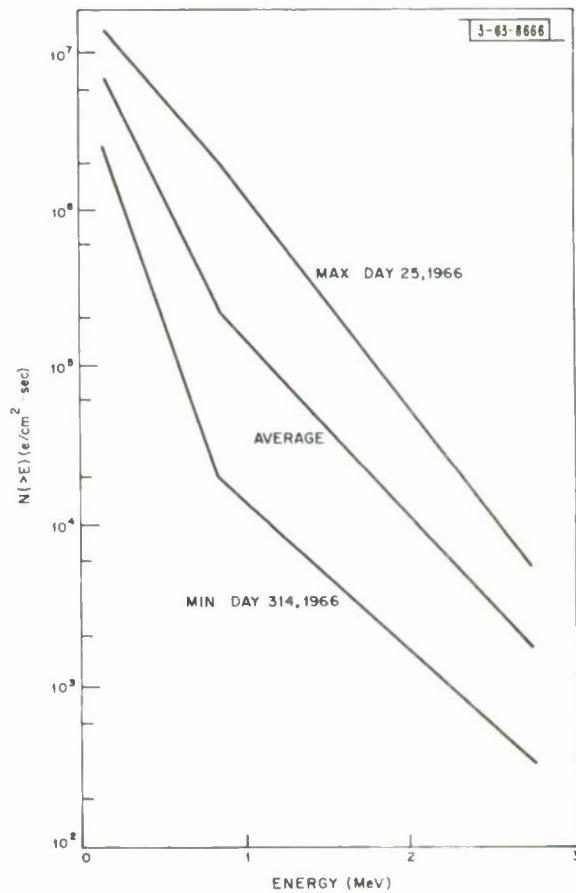
Fig. 4. Omnidirectional electron flux integral spectrum (based on calculations by J. I. Vette on OGO-A spectrometer data).
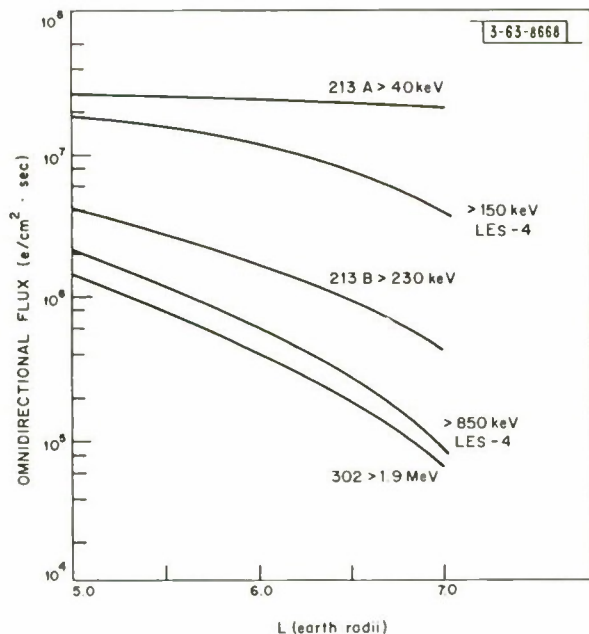
Fig. 5. Variation of electron flux with L.
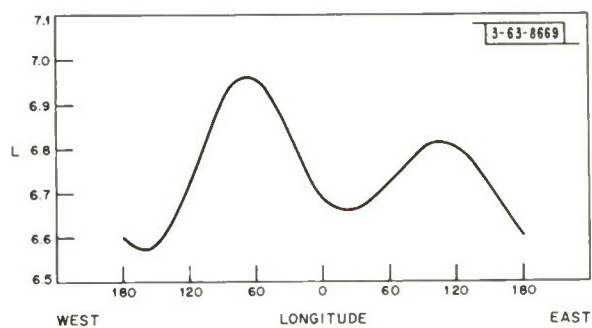
Fig. 6. Variation of L with longitude at R_0 = 6.6.
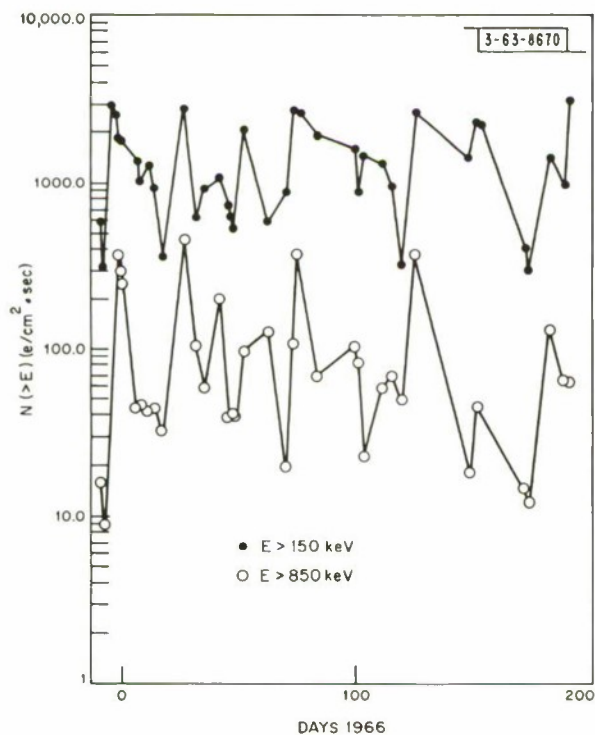
Fig. 7. Temporal variations seen by LES-4 from 21 December 1965 to 8 July 1966.
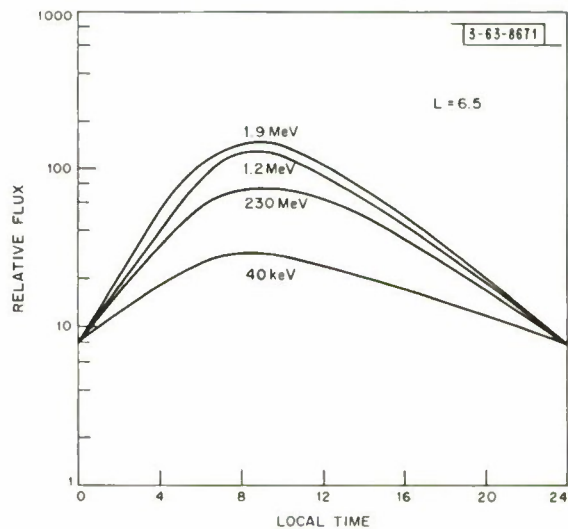
Fig. 8. Composite local time variation (taken from Ref. 15).
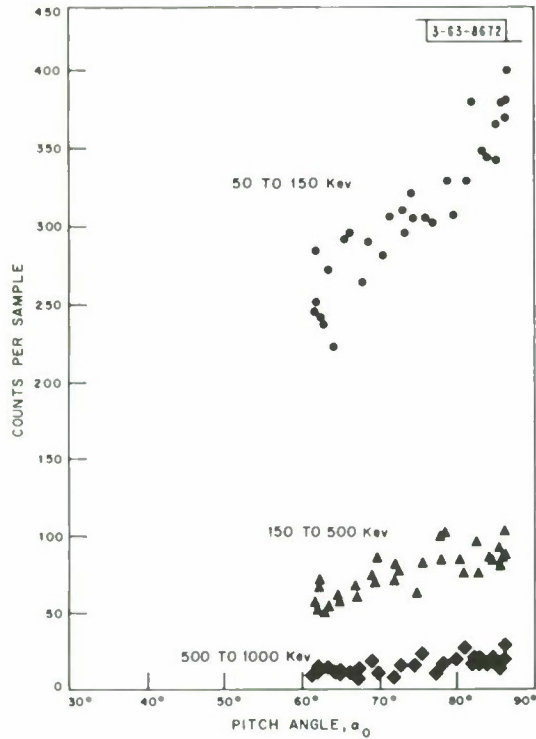
Fig. 9. Pitch angle distribution af electrons in synchronaus arbit (taken from T.W. Lezniak, et ol., Ref. 6).
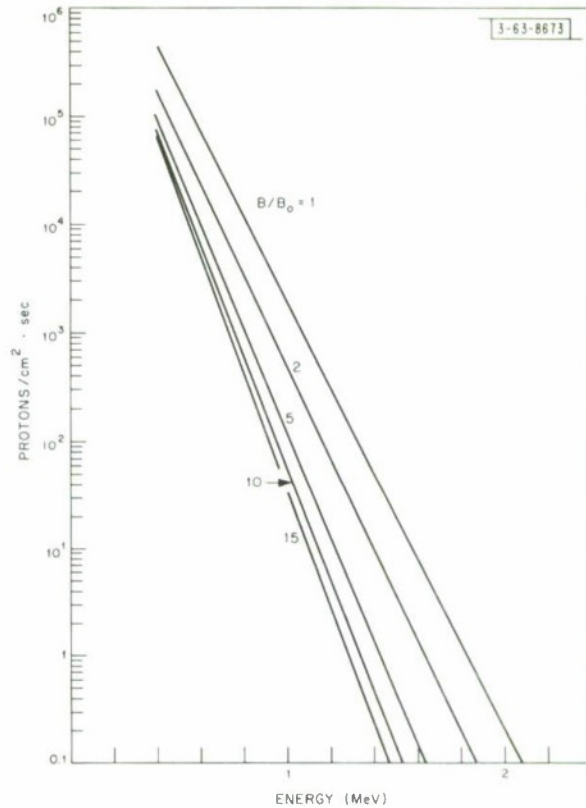
Fig. 10. Integral spectrum of tropped protons in synchranous orbit (data abtoined fram J. H. King, Ref. 55).

Fig. 11. Omnidirectionol proton flux integrol spectrum (based an calculatians by J. I. Vette on data by L. R. Dovis and J.M. Williamson, Ref. 52).
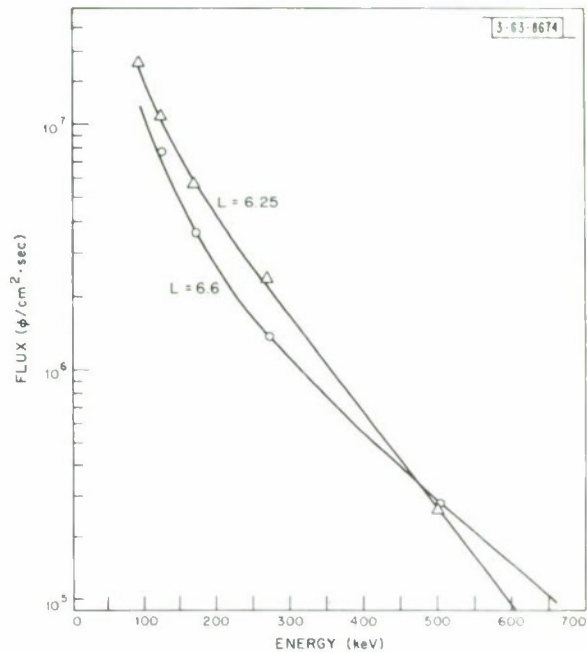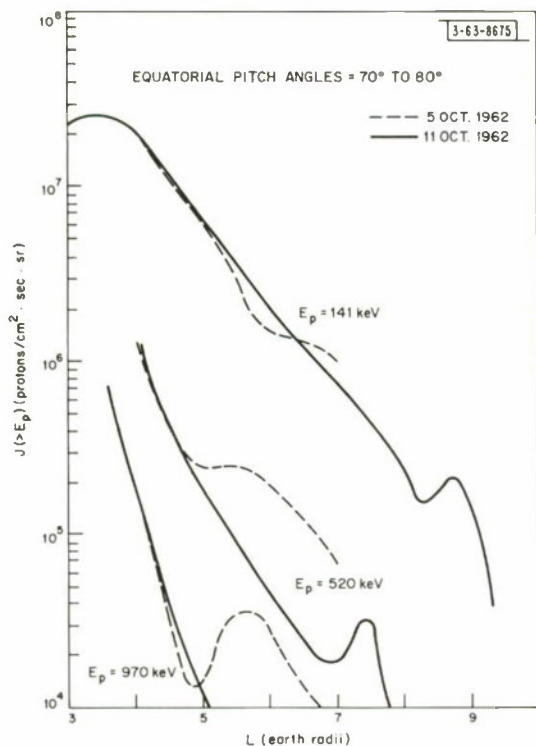
Fig. 12. Effect of solar event of 5 October 1962 on trapped proton distribution (taken from L. R. Davis and J. M. Williamson, Ref. 52, Fig. 11).
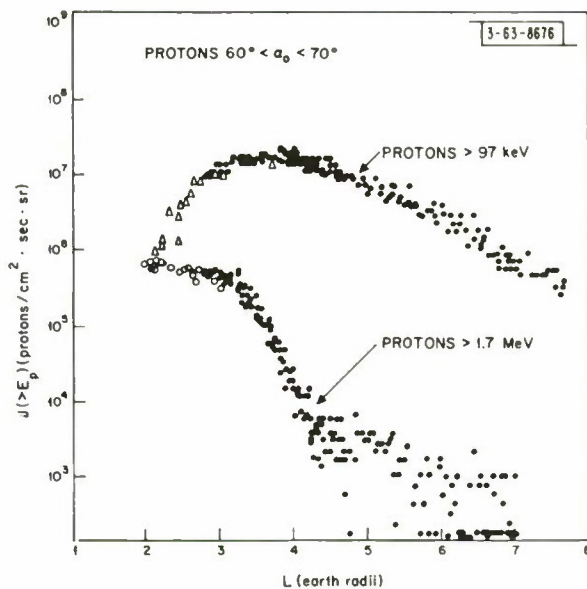
Fig. 13. Temporal variation of trapped proton intensities measured on Explorers 14 and 15 (taken from L. R. Davis, Ref. 51, Fig. 12).
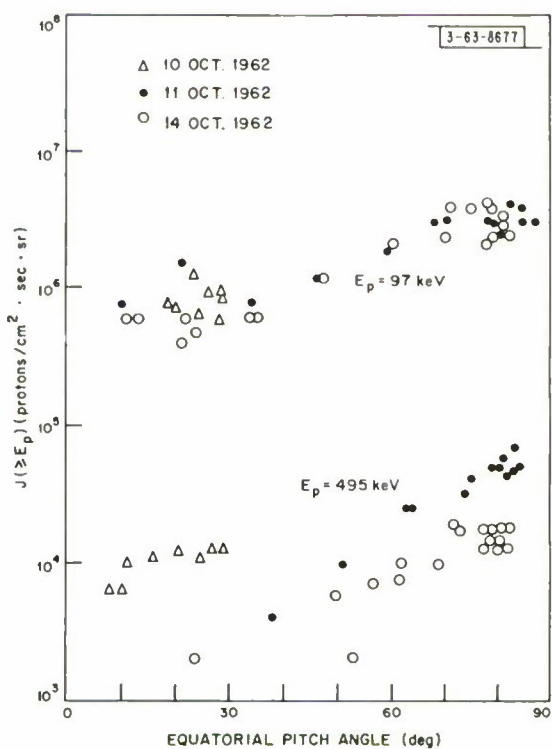
Fig. 14. Equatorial pitch-angle distribution of trapped protons at L = 6 (taken from L. R. Davis, Ref. 51, Fig. 8).
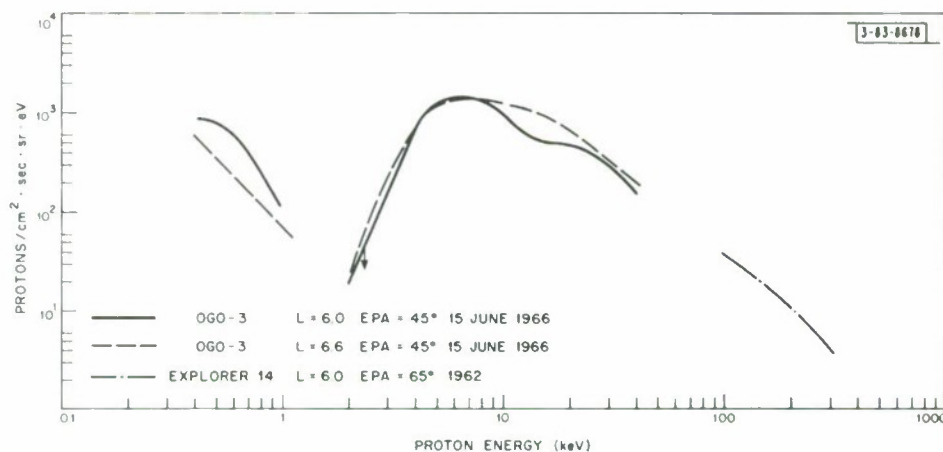
Fig. 15. Differential energy spectrum of low energy trapped protons (based on data from L. A. Frank, Ref. 39 and L. R. Davis, Ref. 51).
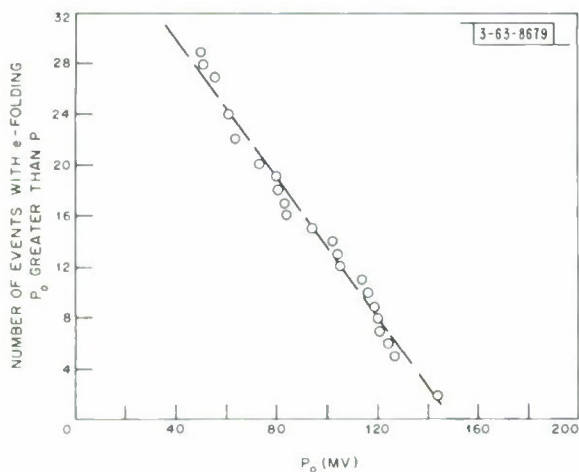
Fig. 16. Integrated P_0 distribution for solar-flare events (taken from W. R. Webber, Ref. 67, Fig. 19).
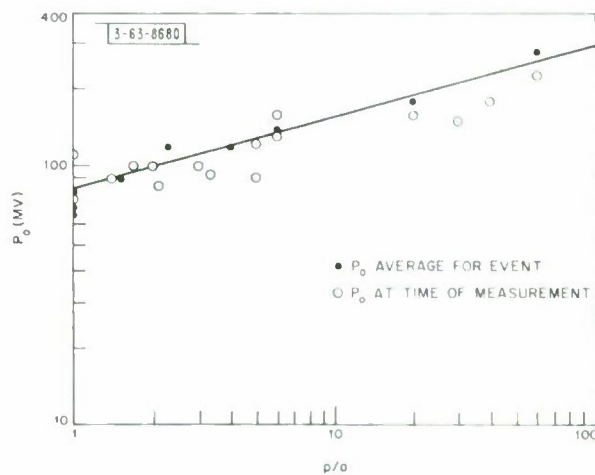
Fig. 17. Proton-to-alpha-particle ratio as a function of characteristic rigidity P_0 (taken from W. R. Webber, Ref. 65, Fig. 3).
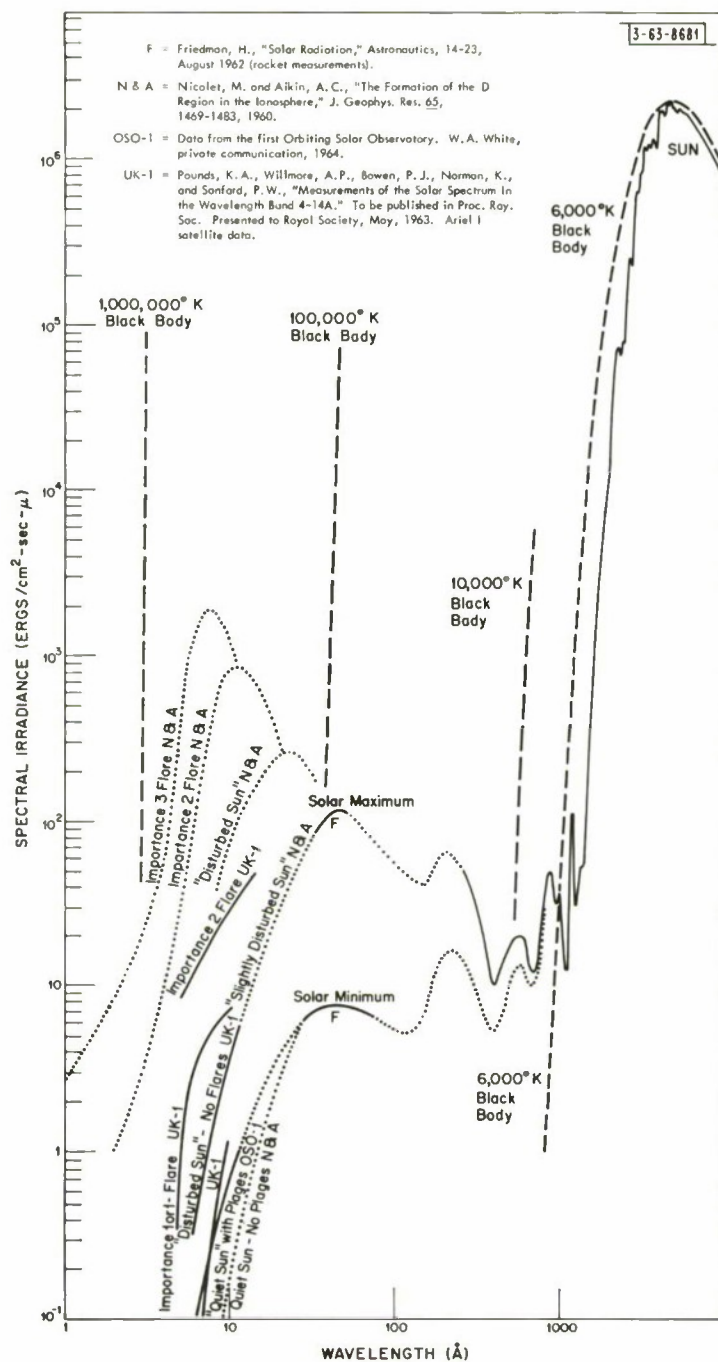
Fig. 18. Solar x-ray spectrum (taken from H. H. Malitsan, Ref. 88).

Fig. 19. Integrated annual intensity
of solar particles as a function of
average yearly sunspot number (based
on data from W.R. Webber, Ref. 65).
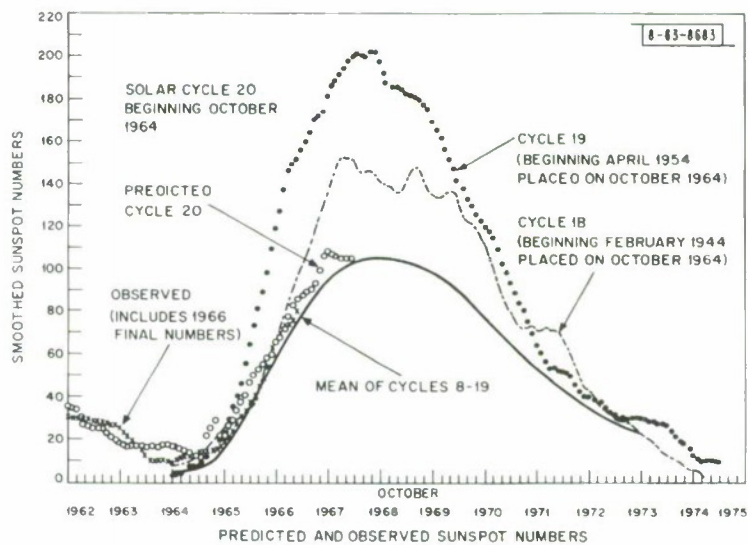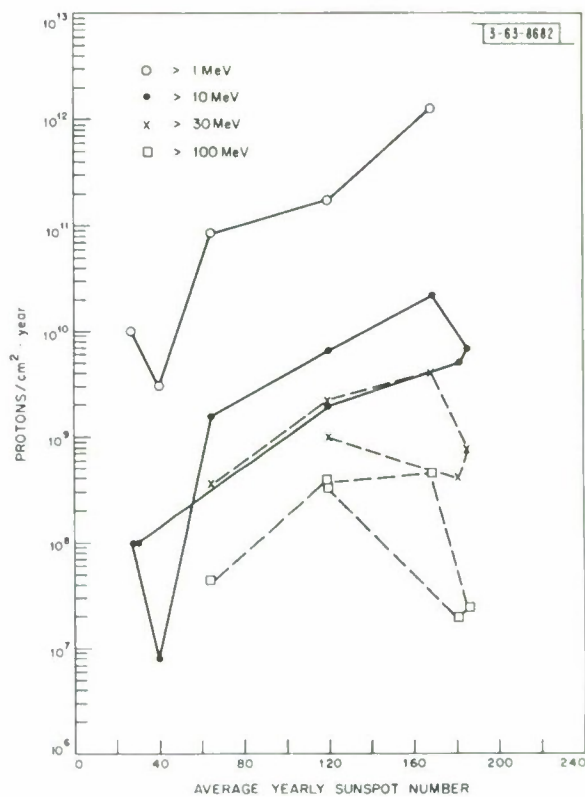
Fig. 20. Predicted and observed sunspot numbers (taken from Ref. 97).

MEAN COUNTS PER SEC

10,000

3-03-8684

E > 150 keV

1000

100

E > 850 keV

10

PROTONS

1

300   344   429   513   558   682   721   805   850

TIME

5.174   5.739   6.122   6.337   6.383   6.273   5.947   5.354   4.329
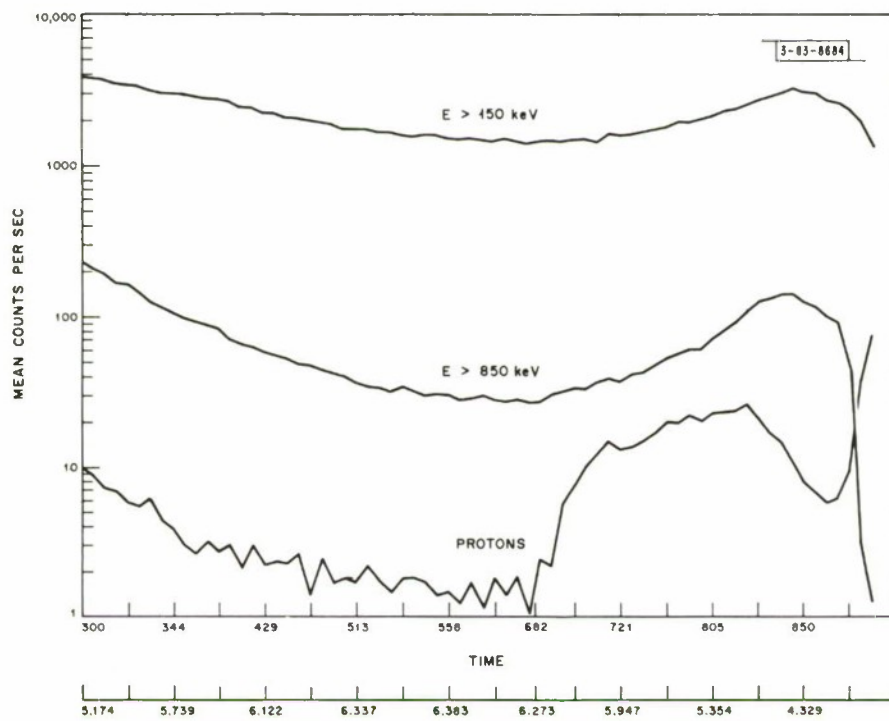
Fig. 21.   Penetration of flare particles into the magnetosphere.
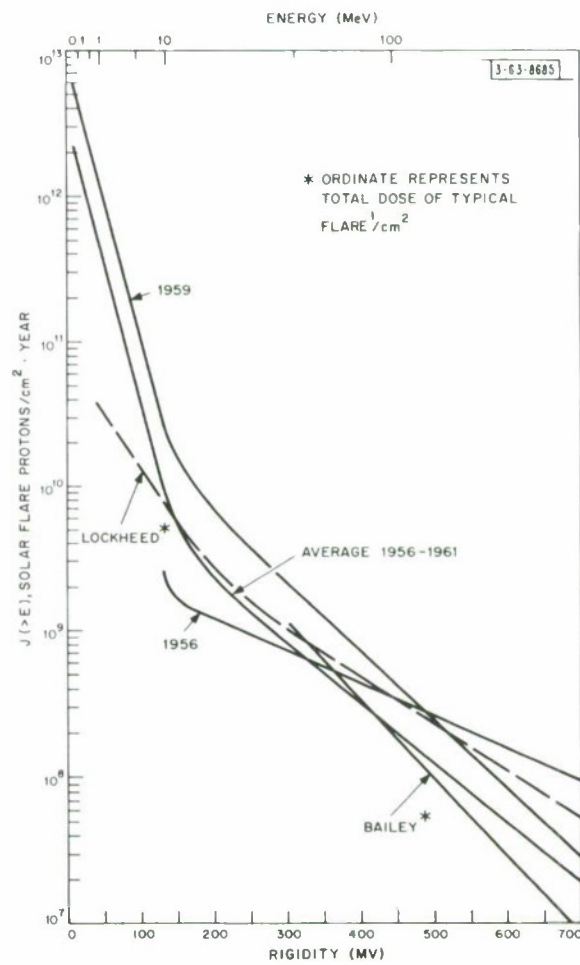
Fig. 22. Integrol onnual solar proton intensity vs rigidity.
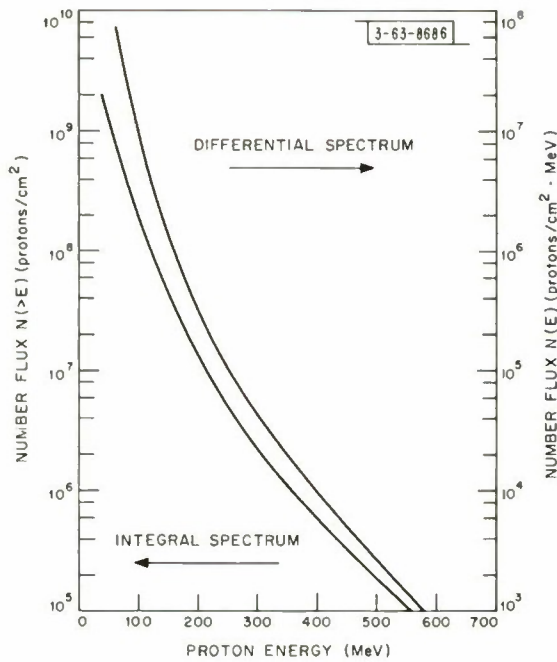
Fig. 23. Differential and integral proton spectra for Bailey's typical solar flare (taken from J.W. Keller, Ref. 110).

Fig. 24. Integral proton flux for a typical large flare (taken from Ref. 111).
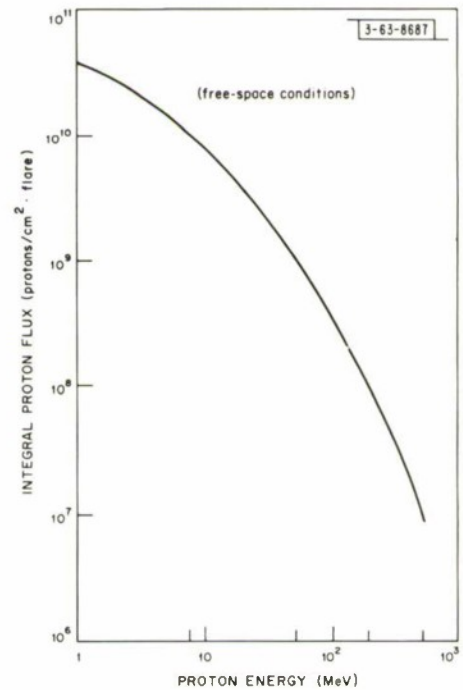
Fig. 25. Predicted integrated solar flare proton spectra.
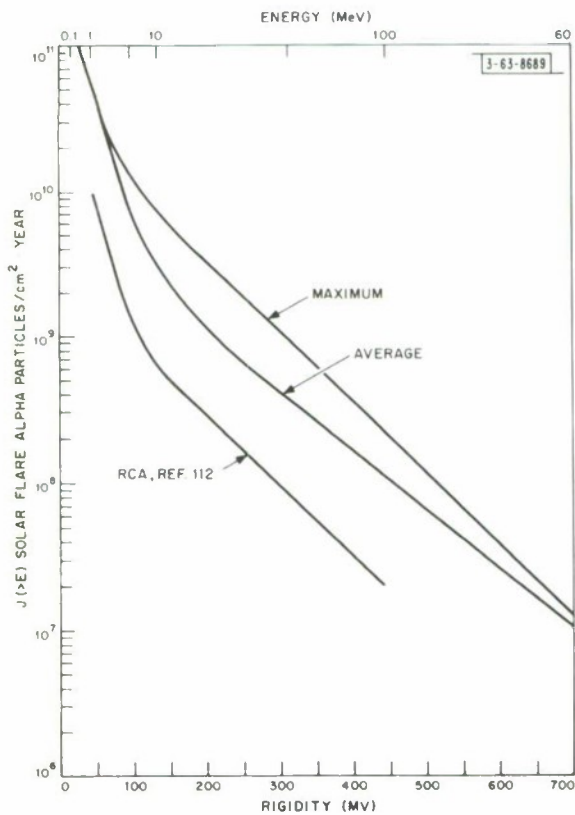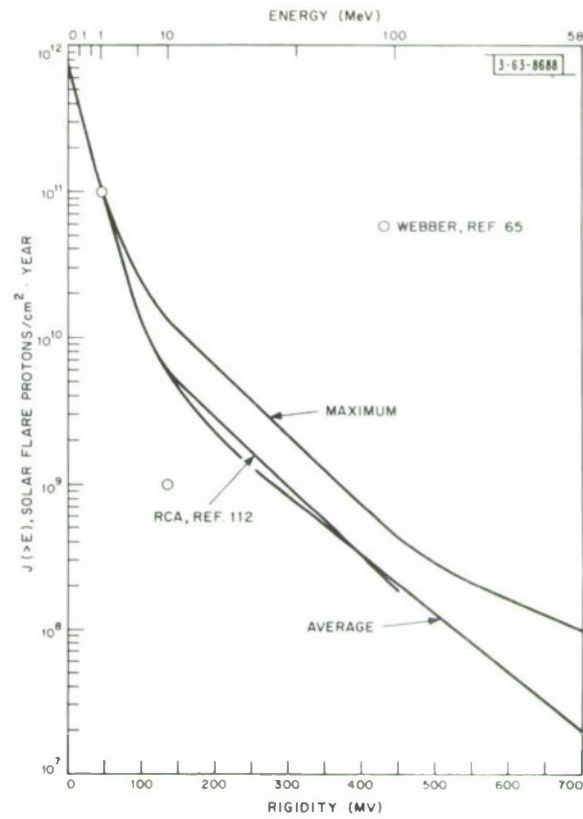
Fig. 26. Predicted integrated solar flare alpha particle spectra.
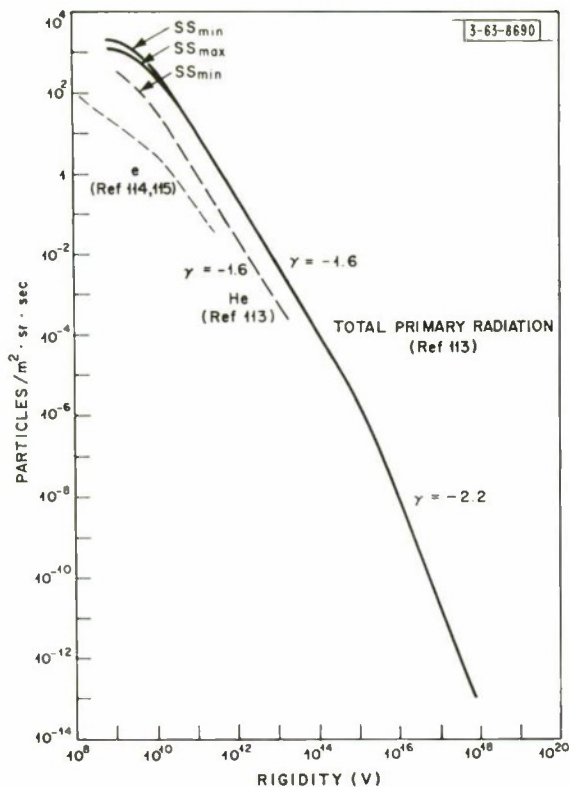
Fig. 27. Integral spectrum of galactic cosmic rays (total primary radiation and helium nuclei from W.R. Webber, Ref. 113, electrons from C.J. Waddington, Ref. 114 and P. Meyer, Ref. 115).
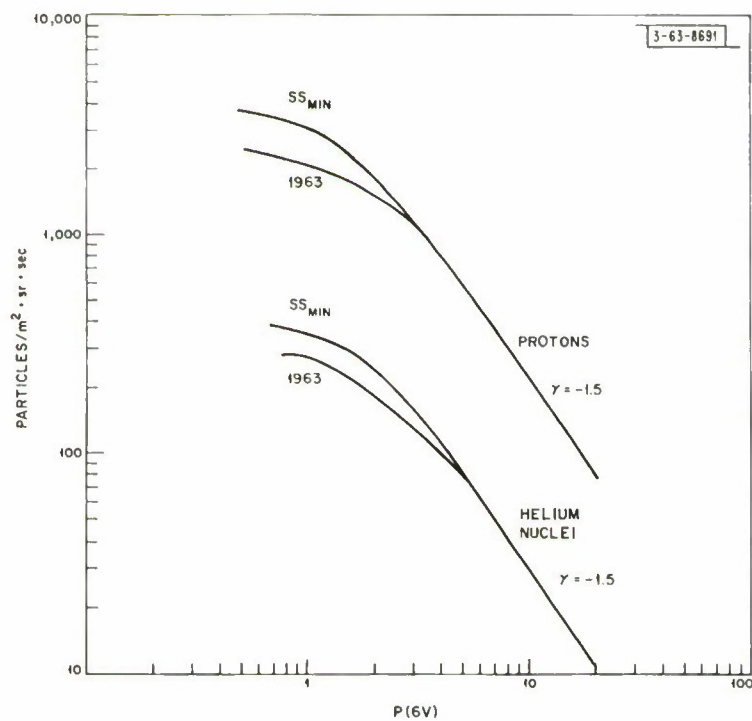
Fig. 28. Integral spectra of galactic cosmic rays (taken from J.F. Ormes and W.R. Webber, Ref. 116).

Fig. 29. Differentiol spectro of goloctic cosmic rays ot low rigidities (protons ond helium nuclei 1963 from W.R. Webber ond J.F. Ormes, Refs. 113, 116; protons and helium nuclei 1965 from V.K. Bolosubrohmonyon, et al., Ref. 117; electrons 1964 from J. L'Heureux ond P. Meyer, Ref. 118).
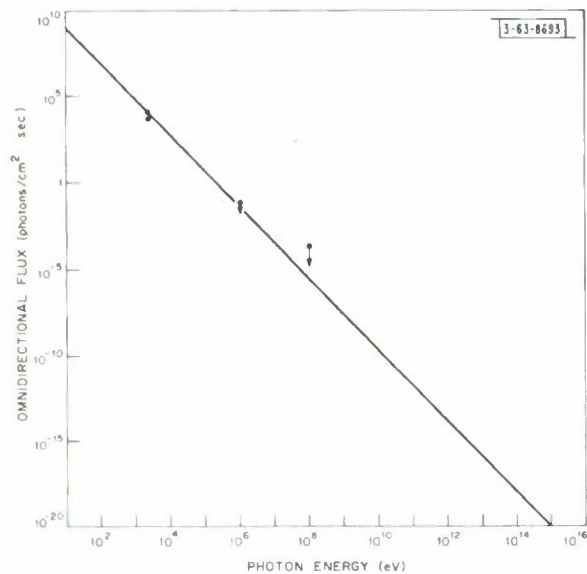

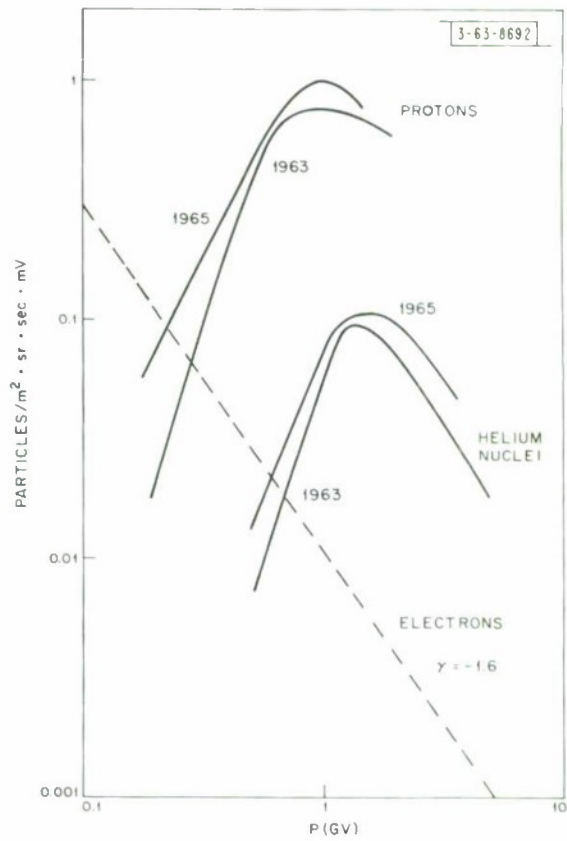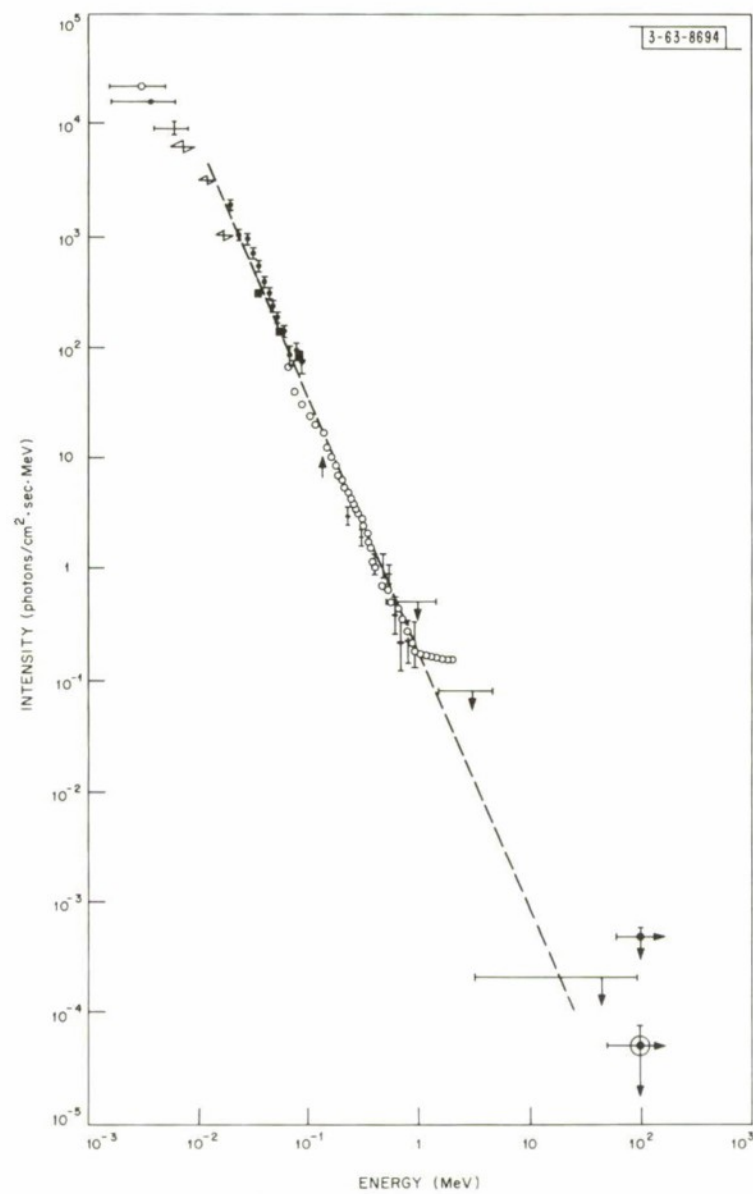Fig. 30. High energy cosmic ray photon spectrum (taken from R.J. Gould and G.R. Burbidge, Ref. 122).

Fig. 31. Differential cosmic ray photon spectrum (taken from R. Rocchia, et al., Ref. 132).

DOCUMENT CONTROL DATA – R&D

(Security classification of title, body of abstract and indexing annotation must be entered when the overall report is classified)

1. ORIGINATING ACTIVITY (Corporate author)	2a. REPORT SECURITY CLASSIFICATION
Lincoln Laboratory, M.I.T.	Unclassified
	2b. GROUP None

3. REPORT TITLE

Charged Particle Radiation Environment in Synchronous Orbit

4. DESCRIPTIVE NOTES *(Type of report and inclusive dates)*

Technical Report

5. AUTHOR(S) *(Last name, first name, initial)*

Stanley, Alan G. and Ryan, Jean L.

6. REPORT DATE	7a. TOTAL NO. OF PAGES	7b. NO. OF REFS
15 May 1968	56	132

8a. CONTRACT OR GRANT NO. AF 19 (628)-5167	9a. ORIGINATOR'S REPORT NUMBER(S)
b. PROJECT NO. 649L	Technical Report 443
c.	9b. OTHER REPORT NO(S) *(Any other numbers that may be assigned this report)*
d.	ESD-TR-68-12

10. AVAILABILITY/LIMITATION NOTICES

This document has been approved for public release and sale; its distribution is unlimited.

11. SUPPLEMENTARY NOTES	12. SPONSORING MILITARY ACTIVITY
None	Air Force Systems Command, USAF

13. ABSTRACT

The present state of knowledge of the charged particle radiation environment in synchronous orbit is described. The composition, intensity, energy spectrum and temporal variations of the radiation are listed. The data are based on measurements on board satellites in elliptical and in synchronous orbits, including the results from the electron telescope on board LES-4, whose apogee is in synchronous orbit. The radiation consists mainly of trapped electrons and low energy protons, but solar flare protons also make a significant contribution. The time-averaged data are given in a form useful for predicting the long-term radiation environment to which a satellite in synchronous orbit would be exposed.

14. KEY WORDS

charged particles	space environment	solar flares
Van Allen radiation belt	cosmic rays	solar protons